Divergent immunometabolic changes in adipose tissue and skeletal muscle with ageing in healthy humans

Trim, Will; Walhin, Jean-Philippe; Koumanov, Francoise; Bouloumie, Anne; Lindsay, Mark; Chen, Yung Chih; Travers, Rebecca; Turner, James; Thompson, Dylan

[Link to publication on Research at Birmingham portal](#)

Divergent immunometabolic changes in adipose tissue and skeletal muscle with ageing in healthy humans

William V. Trim[1,4] , Jean-Philippe Walhin[1], Françoise Koumanov[1] , Anne Bouloumié[2],
Mark A. Lindsay[3], Yung-Chih Chen[1,5], Rebecca L. Travers[1], James E. Turner[1] and Dylan Thompson[1]

[1]*Department for Health, Centre for Nutrition, Exercise, and Metabolism, University of Bath, Bath, Somerset, UK*
[2]*INSERM UMR1048, Université Paul Sabatier, I2MC, Toulouse, France*
[3]*Department of Pharmacy and Pharmacology, University of Bath, Bath, Somerset, UK*
[4]*Department of Immunology and Biochemistry at Trinity College Dublin, Dublin, Ireland*
[5]*Department of Physical Education at the National Taiwan Normal University, Taipei, Taiwan*

Key points

- Ageing is associated with increased systemic inflammation and metabolic dysfunction that contributes to the development of age-associated diseases.
- The role of adipose tissue in immunometabolic alterations that take place with ageing is unknown in humans.
- We show, in healthy, active and lean older adults, that adipose tissue, but not skeletal muscle, displays considerable pro-inflammatory transcriptomic, cellular and secretory changes, as well as a reduction in insulin signalling proteins compared to younger adults.
- These findings indicate that adipose tissue undergoes substantial immunometabolic alterations with ageing, and that these changes are tissue-specific and more profound than those observed in skeletal muscle or in the circulation.
- These results identify adipose tissue as an important tissue in the biological ageing process in humans, which may exhibit signs of immunometabolic dysfunction prior to systemic manifestation.

Abstract   Ageing and obesity are both characterized by inflammation and a deterioration in metabolic health. It is now clear that adipose tissue plays a major role in inflammation and metabolic control in obesity, although little is known about the role of adipose tissue in human ageing. To understand how ageing impacts adipose tissue, we characterized subcutaneous adipose tissue and skeletal muscle samples from twelve younger (27 ± 4 years [Young]) and twelve older (66 ± 5 years [Old]) active/non-obese males. We performed a wide-range of whole-body and tissue measures, including RNA-sequencing and multicolour flow cytometry. We also measured a range of inflammatory and metabolic proteins in the circulation and their release by adipose tissue,

William Trim received his PhD in 2019 from the University of Bath (UK) under the supervision of Professor Dylan Thompson. His PhD investigated the impact of physical inactivity and ageing on adipose tissue, skeletal muscle, and systemic inflammatory and metabolic health. His PhD was part of an international collaboration with the European Space Agency and the I2MC institute (Toulouse, France) investigating the effect of long-term bed rest on human adipose tissue. He is currently a postdoctoral researcher in the Lynch Lab across Trinity College Dublin (Ireland) and Harvard University (USA) characterizing multiple human adipose tissue depots in health and disease.
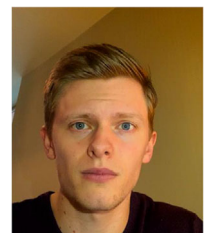
ex vivo. Both adipose tissue and muscle had ∼2-fold more immune cells per gram of tissue with ageing. In adipose tissue, this immune cell infiltration was driven by increased memory/effector T-cells, whereas, in muscle, the accumulation was driven by memory/effector T-cells and macrophages. Transcriptomic analysis revealed that, with ageing, adipose tissue, but not muscle, was enriched for inflammatory transcripts/pathways related to acquired and innate immunity. Ageing also increased the adipose tissue pro-inflammatory secretory profile. Insulin signalling protein content was reduced in adipose tissue, but not muscle. Our findings indicate that adipose tissue undergoes substantial immunometabolic changes with ageing in humans, and that these changes are tissue-specific and more profound than those observed in the circulation and skeletal muscle.

Corresponding author D. Thompson: Department for Health, Centre for Nutrition, Exercise and Metabolism, University of Bath, Bath, Somerset, BA2 7AY, UK. Email: d.thompson@bath.ac.uk

Introduction

Ageing is accompanied by dysregulation of a variety of biological systems (Lopez-Otin *et al.* 2013) and is characterized by sarcopenia, whole-body metabolic dysfunction and low-grade chronic inflammation (Pérez *et al.* 2016; Franceschi *et al.* 2018). It has been proposed that adipose tissue may become dysfunctional with advancing age and play a role in the development of age-related morbidities (Pérez *et al.* 2016). Adipose tissue is an endocrine organ that produces a wide array of adipokines from either adipocytes and/or the immune/non-haematopoietic stromal vascular fraction (SVF). Adipokines affect a range of physiological processes involved in the regulation of energy balance and inflammation and also influence the function of other organs via endocrine action (Fantuzzi, 2005; Trim *et al.* 2017). In the context of obesity, the link between metabolic and inflammatory dysfunction in adipose tissue is well established, with stromal cells playing a central role (Trim *et al.* 2018). Adipose tissue dysfunction can occur in response to many stimuli and leads to adipocyte apoptosis, necrosis, fibrosis and hypoxia (Reilly & Saltiel, 2017). These processes contribute to changes in the extracellular matrix, local blood flow and aberrant adipokine secretory profiles, all of which drive local and systemic metabolic and inflammatory perturbations (Hotamisligil, 2006; Trim *et al.* 2017).

Ageing is associated with an altered systemic adipokine profile including reduced adiponectin, and elevated leptin and interleukin (IL)-6 (Mancuso & Bouchard, 2019). These changes could be a result of age-associated adipose tissue dysfunction involving adipocytes and/or adipose SVF, independent of the expansion in absolute adiposity with age (Batsis & Villareal, 2018). In humans, during ageing, there is some evidence that adipose tissue macrophages increase in number and pro-inflammatory potential, similar to obesity (Ortega Martinez de Victoria *et al.* 2009). However, that study was restricted to a population of Pima Indians with a maximum age of 45 years (Ortega Martinez de Victoria *et al.* 2009). Rodent studies indicate that ageing leads to macrophage accumulation secondary to decreased vascularization and local hypoxia (Soro-Arnaiz *et al.* 2016; Trim *et al.* 2018) and that changes to adipose tissue regulatory T-cells, CD4+/CD8+ T-cells and B-cells contribute to age-associated adipose tissue dysfunction (Lumeng *et al.* 2011; Bapat *et al.* 2015; Frasca & Blomberg, 2017; Camell *et al.* 2019). Moreover, a recent proteomics analysis of nine tissues in aged mice revealed altered adipose tissue inflammation and metabolism as a key signature of organismal ageing (Yu *et al.* 2020). However, little is known about the impact of ageing on adipose tissue function in humans beyond 45 years, as well as how changes in adipose tissue are linked to whole-body metabolic and inflammatory health or changes in other tissues that are impacted by age, such as skeletal muscle (Pillon *et al.* 2013; Dalle *et al.* 2017; Yang & Hu, 2018).

The present study aimed to characterize inflammatory and metabolic changes in subcutaneous adipose tissue that occur with ageing, as well as compare these changes to those in muscle and blood in younger and older, non-obese adults. Collectively, this will provide vital information on the ætiology of age-related chronic inflammatory diseases and potentially aid in the identification of therapeutic targets against age-related diseases.

Methods

Experimental design and ethical approval

One-hundred and nine individuals undertook preliminary screening, from which 24 males aged 20–35 years ($n = 12$; Young) and 60–85 years ($n = 12$; Old) years

participated based on predetermined eligibility criteria. Participants were recruited by local advertisement. The protocol was reviewed and approved by the South West, Bristol Central NHS Research Ethics Committee (REC reference: 16/SW/0003), was registered on *ClinicalTrials.gov* (NCT02777138) and was conducted in accordance with the *Declaration of Helsinki*. All participants provided their written informed consent. Participant recruitment was conducted between August 2016 and March 2018. Participant data was assigned identifying codes within respective groups, without blinding from group allocation.

Briefly, participants attended the laboratory for a preliminary assessment, including body composition, resting metabolic rate and anthropometric measures. Following this initial visit, potential participants had their physical activity levels monitored across seven consecutive days using a multisensor physical activity monitor and also completed weighed food and fluid records across 3 days. Participants meeting eligibility criteria following these initial assessments attended the laboratory on one more occasion (main experimental visit) to undergo fasted blood sampling, as well as provide adipose tissue and skeletal muscle biopsies, followed by a 3 h meal tolerance test.

Participant eligibility

To be eligible for the study, participants were required to have a physical activity level (PAL) in the range 1.4−1.9 and fat mass index (FMI) in the range 4−8 kg m^{-2}. The range of PAL was used to capture individuals who were low-to-moderately active (Brooks *et al.* 2004; FAO/WHO/UNU, 2005) to control for the effect physical activity has on adipose tissue physiology (Thompson *et al.* 2012). The range of FMI was used to include individuals who were lean to moderately overweight to avoid the effects of excess adiposity on adipose tissue inflammation (Travers *et al.* 2015).

Individuals were excluded if they self-reported any of the following: diagnosed medical condition; taking medications known to interfere with immune function or lipid/glucose metabolism; taking analgesic or anti-inflammatory medication; prior negative reactions to lidocaine anaesthetic; regularly undertaking heavy resistance exercise; smokers; or not weight stable for the past 3 months (i.e. weight change ± 3 %).

Preliminary assessments

Resting energy expenditure was determined between 08.30 and 09.00 h via indirect calorimetry as described previously (Frayn, 1983). Briefly, participants rested for 15 min before measurements were taken. The percentage of O_2 and CO_2 in expired air samples was determined using paramagnetic and infrared gas analysers, respectively (Series 1400; Servomex Ltd, Crowborough, UK). This process was repeated a minimum of four times. A mean of two or three recordings made within 100 kcal of one another was assigned as the resting metabolic rate (RMR) (Betts, 2012).

Body composition was determined using dual-energy X-ray absorptiometry (DEXA) (Discovery; Hologic, Marlborough, MA, USA). FMI (Kelly *et al.* 2009) and central fat mass (fat mass between L1 and L4 vertebrae) were also determined (Paradisi *et al.* 1999; Travers *et al.* 2015). Waist-hip ratio was calculated according to guidelines from the World Health Organization (WHO, 2011).

Participants were fitted with a multisensor physical activity monitor (SenseWear; Bodymedia, Pittsburgh, PA, USA) for seven consecutive days to determine habitual physical activity levels. Data were uploaded onto SenseWear Professional, version 8.0.0 (Bodymedia) for analysis. PAL was quantified using SenseWear Professional, version 8.0.0, and categorized according to Brooks *et al.* (2004) and FAO/WHO/UNU (2005) guidelines. Individuals recording a PAL between 1.4−1.9 (low-to-moderately active) (Brooks *et al.* 2004; FAO/WHO/UNU, 2005) were eligible for participation. Total energy expenditure (TEE) was then calculated as a product of recorded estimates of activity energy expenditure + RMR + diet induced thermogenesis (estimated at 10 % of TEE) (Westerterp, 2004).

Dietary analysis

Three day (two weekdays and one weekend day) weighed food and fluid records were collected during the 7 day activity monitoring period to assess habitual dietary intake. Participants recorded food mass (g) and fluids consumed (mL) pre- and post-meal on digital scales accurate to 1 g (Salter, Tonbridge, UK). Food and fluid records were analysed using Nutritics software (Nutritics, Dublin, Ireland).

Main experimental visit

Participants were required to refrain from performing any strenuous physical activity for 48 h, and from consuming alcohol or caffeine for 24 h prior to the main trial, which was confirmed verbally. Visit days were scheduled so as to ensure participants had been free from self-reported illnesses for >2 weeks and from vaccinations for >4 weeks (Huang *et al.* 1992).

Individuals were asked to attend the laboratory between 08.00 and 09.00 h after fasting for a minimum of 10 h and to consume one pint of water upon waking to normalize

hydration status. Following a 15 min rest in the supine position, fasted blood samples were drawn followed by adipose tissue and skeletal muscle biopsies. Following these procedures, participants consumed a mixed-meal drink and blood samples were drawn at regular intervals for 3 h following consumption to assess the metabolic response to a meal challenge.

Blood sampling

Venous blood samples were collected from an antecubital vein. Samples for serum separation were rested at room temperature for 30 min prior to centrifugation at $3000 \times g$ for 10 min at 4°C. Plasma samples were immediately centrifuged upon collection and stored at −80°C until analysis. Peripheral blood mononuclear cells (PBMCs) were isolated by density gradient separation (Ficoll; Greiner Bio-One, Stonehouse, UK) in Leucosep tubes (Greiner Bio-One Ltd., Gloucestershire, UK) for fresh analysis on the day of collection.

Adipose tissue sampling

Subcutaneous adipose tissue samples were obtained from ∼5 cm lateral to the umbilicus with a 14 G needle using the needle aspiration method (Travers *et al.* 2015) under local anaesthesia (1 % lidocaine hydro-chloride; Hameln Pharmaceuticals, Gloucester, UK). Visible connective tissue, blood and vasculature were removed with scissors prior to washing the remaining tissue with 0.9 % NaCl solution (B.Braun, Sheffield, UK) over a single-use sterile 100 μm gauze to further clean the sample of contaminating blood. Adipose tissue was portioned dependent on sample size for trans-criptomic analysis (∼100 mg); *ex vivo* culture (3−4 × ∼25 mg) for 3 h to assess basal secretory profiles; enzymatic digestion (250−500 mg) to separate the SVF and mature adipocytes; and immunoblotting. Adipocytes isolated during SVF isolation procedures were harvested and placed into Dulbecco's modified Eagle's medium (DMEM) containing 10 % foetal bovine serum (FBS) and were partitioned for microscopy analysis and insulin stimulation. Tissue partitioned for transcriptomic and immunoblotting analyses was snap-frozen in liquid nitrogen and stored at −80°C until analysis.

Skeletal muscle sampling

Skeletal muscle was obtained from the *Vastus Lateralis* of the dominant leg under local anaesthesia using the Bergström technique (Bergström *et al.* 1967). Samples were partitioned for transcriptomic and immunoblotting

analysis (30−50 mg) and enzymatic digestion to iso-late the SVF for flow cytometry (60−100 mg). Tissue partitioned for transcriptomic and immunoblotting analyses was snap-frozen in liquid nitrogen and stored at −80°C until analysis.

Mixed-meal tolerance test

To examine metabolic control, participants consumed a formulated mixed-meal beverage following the completion of adipose tissue and skeletal muscle biopsy procedures. A standardized mixed-meal test was chosen to produce a physiological response similar to that of a conventional meal (Travers *et al.* 2017). This beverage was formulated in-house, proportional to body mass for consistency across participants, equating to 2 g kg^{-1} body mass (BM) carbohydrate, 0.8 g kg^{-1} BM fat and 0.4 g kg^{-1} BM protein, as used previously (Travers *et al.* 2017). The beverage consisted of whey protein (MyProtein, Cheshire, UK), Elmlea double cream (Elmlea, Exeter, UK), maltodextrin (MyProtein), and 1 pint of whole milk as standard across participants, with five drops of vanilla flavouring (MyProtein). Venous blood was collected immediately following the consumption of the beverage and every 15 min for 90 min, followed by every 30 min thereafter until 180 min post-consumption.

Adipose tissue culture

Adipose tissue was cultured *ex vivo* in sterile culture plates (Nunc, Roskilde, Denmark), at a final concentration of 50 mg of tissue per millilitre in endothelial cell basal medium (PromoCell, Heidelberg, Germany) supplemented with 0.1 % fatty acid-free bovine serum albumin (BSA) and 100 U mL penicillin and 0.1 mg mL^{-1} streptomycin (Sigma-Aldrich, Gillingham, UK). Cultures were maintained at 37 °C, 5 % CO$_2$, and 95 ± 5 % relative humidity (MCO-18A1C CO$_2$ incubator; Sanyo, Osaka, Japan) for 3 h, as described previously (Travers *et al.* 2017). Explant media were collected and stored at −80 °C until analysis.

Adipose tissue digestion

Adipose tissue (250 to 500 mg) was digested using 250 U mL^{-1} type-I collagenase (Worthington Biochemical, Lakewood, NJ, USA) in PBS containing 2 % BSA (pH 7.4) for 45−60 min in a shaking water bath (225 r.p.m) at 37 °C as described in Travers *et al.* (2015). Digestions were terminated by the addition of two volumes of PBS supplemented with 10 % FBS. Isolated adipocytes were recovered by flotation and the SVF cells were then recovered following centrifugation at $700 \times g$ for 5 min.

Adipocyte insulin stimulation and microscopy

Isolated adipocytes were incubated at 37°C and 5 % CO_2 in DMEM supplemented with 10 % FBS, whereupon a fraction was serum-starved in 1 mL of unsupplemented DMEM for 30 min and then incubated with or without 100 nM of insulin for 30 min. Cells were then washed twice with PBS and snap frozen in liquid nitrogen and stored at −80°C until analysis.

A portion of isolated adipocytes was placed onto a glass slide and cover slip for imaging under a light microscope (Olympus, Tokyo, Japan). Adipocyte diameters were measured using ImageJ (National Institutes of Health, Bethesda, MD, USA) after image file randomization to mask participant grouping. A minimum of 50 adipocytes were measured for each participant (two participants from the Old group were removed for having insufficient adipocytes).

Skeletal muscle digestion

Between 35 and 100 mg of skeletal muscle was placed into 5 mL of DMEM (low glucose, with Glutamax; GIBCO, Fisher Scientific, Waltham, MA, USA) at 37°C in a 60 mm Petri dish. Visible signs of blood were washed away by passing samples into successive Petri dishes containing fresh DMEM. Cleaned tissue was digested enzymatically using the method described in Girousse *et al.* (2019). Following the unexpected discovery that the CD4 surface protein was cleaved by Dispase II, which we retrospectively found had been documented previously (Abuzakouk *et al.* 1996); this protocol was subsequently modified. All remaining skeletal muscle digestions [$n = 10$ (Young) and 5 (Old)] were digested with only collagenase B (0.5 U mL^{-1}) in DMEM for 1 h at 37°C and 5 % CO_2 with slow agitation. Digested samples were then exposed to ACK lysis buffer (Thermo Fisher, Leicester, UK) for 1 min, washed in FACS buffer (PBS with 2 % FBS and 2 mM EDTA) followed by filtration through a 40 μm cell strainer (Falcon; BD Bioscience, San Jose, CA, USA). This final suspension was centrifuged at 400 × *g* for 7 min at 4°C to pellet off stromal cells which were then put forward for flow cytometry analysis.

Adipose tissue and skeletal muscle RNA isolation

Total RNA (including microRNAs) was extracted from frozen adipose tissue (∼100 mg) or skeletal muscle samples (30–50 mg) using miRNeasy Mini Kit (Qiagen, Crawley, UK) in accordance with the manufacturer's instructions.

Following RNA isolation, samples were DNase treated with TURBO DNase (Thermo Fisher) in accordance with the manufacturer's instructions, followed by phenol–chloroform extraction and ethanol precipitation. The purified RNA pellets were re-suspended in 35 μL of nucleotide-free water each (Thermo Fisher) with 2 μL used for quality control. Thirty microlitres of RNA at a set concentration of 2.1 μg per 30 μL was sent for RNA-sequencing.

Transcriptomic and bioinformatics analyses

RNA-sequencing was performed on RiboZero-treated total RNA, on a HiSeq4000 (Illumina, Inc., San Diego, CA, USA) by the Oxford Genomics Centre (Wellcome Trust, Oxford, UK). In brief, total RNA was quantified using RiboGreen (Invitrogen, Carlsbad, CA, USA) on the FLUOstar OPTIMA plate reader (BMG Labtech GmbH, Aylesbury, UK) and the size profile and integrity analysed on the 2200 or 4200 TapeStation (RNA ScreenTape; Agilent Technologies, Santa Clara, CA, USA). RIN estimates for all samples were between 1.8 and 8.5. Input material was normalized to 200 ng prior to library preparation. Total RNA was depleted of ribosomal RNA using Ribo-Zero rRNA Removal Kit (Epicentre/Illumina, Human; Illumina, Inc.) in accordance with the manufacturer's instructions. Library preparation was completed using NEBNext Ultra II mRNA kit (New England Biolabs Inc., Ipswich, MA, USA) in accordance with the manufacturer's instructions. Libraries were amplified (11 cycles) on a Tetrad (Bio-Rad Laboratories, Hercukes, CA, USA) using in-house unique dual indexing primers (Lamble *et al.* 2013). Individual libraries were normalized using Qubit (Thermo Fisher) and the size profile was analysed on the 2200 or 4200 TapeStation (Agilent Technologies, California, US). Individual libraries were normalized and pooled together accordingly. The pooled library was diluted to ∼10 nM for storage. The 10 nM library was denatured and further diluted prior to loading on the sequencer. Paired end sequencing was performed using a HiSeq4000 75 bp platform (HiSeq 3000/4000 PE Cluster Kit and 150 cycle SBS Kit; Illumina, Inc.), generating a raw read count of >38.5 million reads per sample.

FastQ sequencing files were uploaded to the Galaxy web platform (usegalaxy.org) for quality control analysis. Raw sequencing files were splice-aligned to the *GRCh38/hg38* reference genome using Hisat2 (Pertea *et al.* 2016), with mapping distance <500 kb between reads. Ensembl (Cambridge, UK) was used to annotate sequencing files against the reference genome (Cunningham *et al.* 2019). Expression levels (fragments per kilobase of transcript per million mapped reads) were estimated using Stringtie (Pertea *et al.* 2015). Differential expression analysis was undertaken using Cuffdiff v.7 (Trapnell *et al.* 2012) and Deseq2 (Love *et al.* 2014), using Gencode v.29 as the reference database (GRCh38.p12) (Frankish *et al.* 2018). *P* values were

adjusted for transcriptome-wide false discovery rate (FDR), with an adjusted significance threshold of $q < 0.05$. P values are reported after adjustment, unless otherwise stated. Functional annotation analysis was performed in the database for annotation, visualization and integrated discovery (DAVID) 6.8 (2019 release) (Huang da *et al.* 2009a, 2009b) and Genesis 1.8.1 (Sturn *et al.* 2002). Pathway analysis was performed using Kyoto Encyclopaedia of Genes and Genomes (KEGG) (https://www.genome.jp/kegg) and Gene Ontology (GO) (http://geneontology.org), using a modified Fisher's exact test [EASE (expression analysis systematic explorer)] (Hosack *et al.* 2003) with a significance threshold of $P < 0.05$. As a result of the loss of one sample and the exclusion of another sample which was identified as a statistical outlier by principal component and hierarchical clustering analysis, the final sample size for adipose tissue was $n = 11$ for both Young and Old.

Immunoblotting

Total proteins from biopsies were recovered from the organic phase of QIAzol-treated (Qiagen, Hilden, Germany) tissue samples used for RNA extraction. Organic phases were extracted and processed for western blot analysis as described previously (Walhin *et al.* 2013). Protein content was determined by BCA protein assay (Thermo Fisher). Isolated primary adipocytes recovered during the SVF preparation and treated or not with insulin were thawed on ice and lysed in RIPA buffer ($2 \times$ stock: 10 mM Tris, pH 7.4, 300 mM NaCl; 1 % sodium deoxycholate; 0.2 % SDS; 0.2 % NP-40), supplemented 1:50 with HALT protease inhibitor cocktail ($100 \times$ stock) (Thermo Fisher) and one tablet per 5 mL of $2 \times$ RIPA buffer of PhosSTOP EASYpack phosphatase inhibitor (Roche AG, Basel, Switzerland).

Protein from whole adipose tissue (20 μg), skeletal muscle (30 μg) and isolated adipocytes ($10-15$ μg) was separated by SDS-PAGE and transferred to a nitrocellulose membrane for immunoblot analysis using the following antibodies against the following proteins: actin (Sigma-Aldrich, Poole, UK; #A2066, dilution 1:1000); Akt2 (Cell Signaling Technology, Beverly, MA, USA; #3063, dilution 1:500); phosphoserine-473 Akt (Cell Signaling Technology; #4058, dilution 1:1000); Akt substrate of 160 kDa (AS160) (Millipore, Burlington, MA, USA; #07-741, dilution 1:500); GAPDH (Proteintech, Manchester, UK; #60004-1-Ig, dilution 1:2000); glucose transporter 4 (GLUT4) (Holman *et al.* 1990) (dilution 1:5000); and insulin receptor β-chain (InsRβ) (Santa Cruz Biotechnology, Dallas, TX, USA; #sc711, dilution 1:500). Images were acquired with EPI Chemi II darkroom (UVP, Upland, CA, USA) and bands were quantified using ImageStudio Lite (LI-COR Biosciences, Lincoln, NE, USA).

In fasted plasma, advanced glycated end-products (AGEs) were assessed by immunoblotting with an anti-carboxymethyl lysine antibody (Abcam; Cambridge, UK; ab27684, dilution 1: 1000). Nine microlitres of plasma diluted 1:30 in 100 mM Tris HCL (pH 8.5) and prepared for immunoblotting as detailed above with alterations to the blocking buffer which was a 3 % BSA solution (in PBS), 0.22 μm filtered. Images were acquired with EPI Chemi II darkroom (UVP) and bands were quantified using ImageStudio Lite (LI-COR Biosciences).

Flow cytometry

Samples (250,000 PBMCs or half of the tissue SVF) were incubated with fluorophore-conjugated antibodies in two separate tubes, one for T-cells and another for mono-cytes/macrophages and endothelial/progenitor cells. PBMC, adipose and muscle T-cell panels contained the following antibodies, all purchased from BD Biosciences (Oxford, UK): anti-CD3-PE-Cy7 clone SK7 (#557851, dilution 1:40), anti-CD4-APC clone RPA-T4 (#555349, dilution 1:40), anti-CD8-APC-Cy7 clone SK1 (#557834, dilution 1:40), anti-CD45RA-FITC clone HI100 (#555488, dilution 1:10), anti-CD27-PE clone M-T271 (#555441, dilution 1:10), anti-CD45-V450 clone HI30 (#560367, dilution 1:80) and anti-HLA-DR-V500 clone G46-6 (#561224, dilution 1:40). PBMC mono-cyte, and adipose and muscle macrophage panels contained the following fluorophore-conjugated anti-bodies: anti-CD14-FITC clone M5E2 (#555397, dilution 1:10), anti-CD16-APC-Cy7 clone 3G8 (#555407, dilution 1:80), anti-CD45-V450 clone HI30 (#560367, dilution 1:80), anti-CD206-APC clone 19.2 (#550889, dilution 1:40) and anti-HLA-DR-V500 clone G46-6 (#561224, dilution 1:40). Isotype controls for CD206 (IgG1, κ-APC) (#554681, dilution 1:40) and HLA-DR (IgG2a, κ-V500) (#561221, dilution 1:40). Fluorescence minus-one controls were conducted on CD45, CD45RA, CD27 and CD206 using PBMCs to inform gating strategies. In the adipose tissue and skeletal muscle tubes, satellite, endothelial and progenitor cells were assessed using the following fluorophore-conjugated antibodies; anti-CD15-PE-Cy7 clone HI98 (#551376, dilution 1:40), anti-CD31-PE clone WM59 (#563652, dilution 1:10), anti-CD34-PE-Cy7 clone 581 (#560710, dilution 1:40), anti-CD56-PE clone B159 (#557747, dilution 1:10) and anti-CD140a-PerCP-Cy5.5 clone αR1 (#563575, dilution 1:40). Gating strategies for PBMCs and tissues are detailed in Fig. 1.

To obtain absolute cell counts for PBMC and SVF samples, counting beads (100 μl of Perfect-Count Microspheres; Cytognos, Salamanca, Spain) were added to all experimental samples, in accordance with the manufacturer's instructions. Flow cytometry was performed on a FACSAria III (BD Biosciences) and the
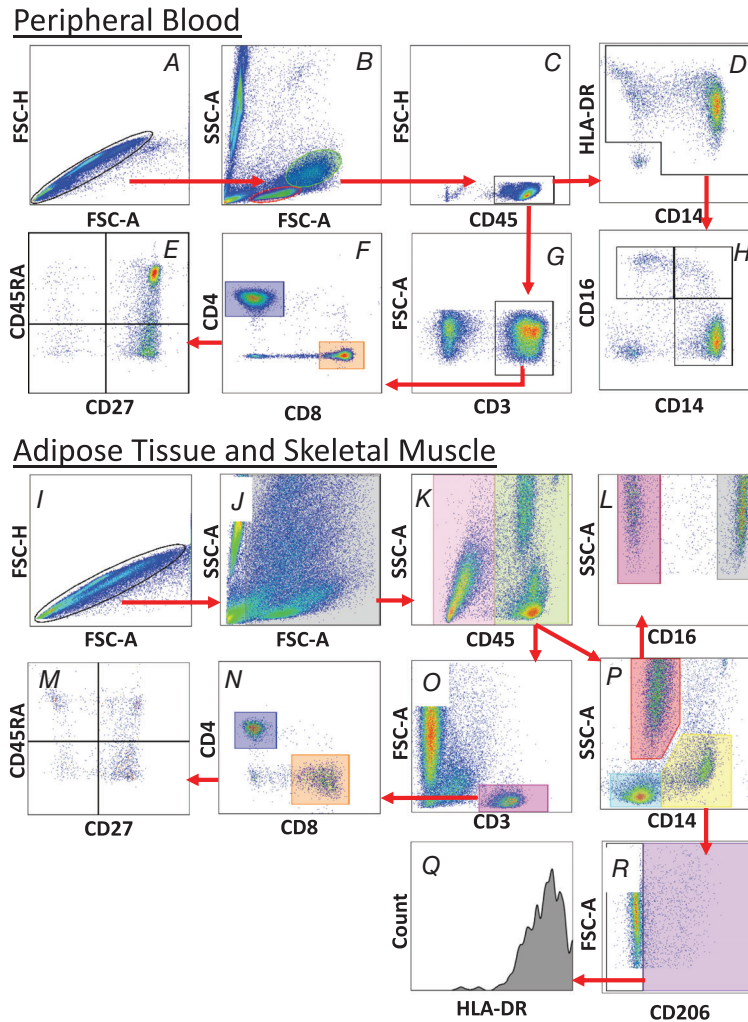
Figure 1. Representative flow cytometry gating profiles in peripheral blood, adipose tissue and skeletal muscle

For the purpose of concision, adipose tissue is used as a representative gating strategy for both adipose tissue and skeletal muscle in (*I*) to (*R*) as a result of their similarity in population distributions. Non-haematopoietic cell gating strategies are presented in Fig. 5*G*. T-cells and monocytes in peripheral blood were gated as follows: first, singlets were gated against FSC-H and FSC-A (*A*). Next, singlets were gated against SSC-A and FSC-H to identify lymphocytes (*B*, red) and monocytes (*B*, green). These, respectfully, were gated against FSC-H and CD45 (*C*) to identify CD45+ leukocytes. From here, monocytes were gated against HLA-DR and CD14 to exclude CD14–HLA-DR^{low} NK-cells (*D*). Non-NK-cells were then gated against CD16 and CD14 to identify monocyte subsets (*H*). Lymphocytes were gated from (*C*) against FSC-A and CD3 to identify CD3+ T-cells (*G*), which were further gated against CD4 and CD8 to identify CD4+ and CD8+ T-cell subsets (*F*, blue and orange, respectively). Each T-cell subset gated in (*F*) was gated against CD45RA and CD27 to further identify CD4+ and CD8+ T-cell naïve (NA), central memory (CM), effector memory (EM) and terminally differentiated effector memory cells (EMRA) subsets (*E*). Lymphocyte and monocyte subsets were further tested for activation status by HLA-DR median fluorescence intensity (MFI). In adipose tissue and skeletal muscle, singlets were first identified by gating FSC-H against FSC-A (*A*), whereupon all events (*J*, grey) were identified by gating SSC-A and FSC-A. Tissue macrophages and granulocytes were identified by taking all viable events from (*J*) and gating SSC-A against CD45 to identify CD45+ leukocytes, which were subsequently gated against SSC-A and CD14 (*P*). For tissue macrophages, SSC-A^{low}CD14+ events (*P*, yellow) were then gated against FSC-A and CD206 to identify CD206+ macrophages (*R*, violet), which were subsequently assessed for HLA-DR MFI (*Q*). Granulocytes were identified in (*P*) as SSC-A^{high}CD14– events (*P*, red), which were subsequently gated against SSC-A and CD16 to broadly identify CD16+ and CD16– granulocytes (*L*, grey and rose, respectively). Tissue T-cells were identified by all CD45+ events from (*K*) and gating against SSC-A and CD3 to identify CD3+ T-cells (*O*), which were then gated against CD4 and CD8 to identify CD4+ and CD8+ T-cell subsets (*N*). CD4+ and CD8+ T-cells were gated against CD45RA and CD27 to identify NA, CM, EM and EMRA CD4+ and CD8+ T-cells (*M*), which were also assessed for activation status by HLA-DR MFI. [Colour figure can be viewed at wileyonlinelibrary.com]

results were analysed using FlowJo, version 10 (FlowJo LLC, Ashland, OR, USA). Adipose tissue SVF samples that were potentially contaminated by peripheral blood were identified using unbiased outlier assessments. Briefly, linear regression modelling (Cook, 1977) was used to identify statistical outliers within respective groups, across all cell types measured. If ≥2 cell types for a given individual (e.g. CD4+ EM and CD8+ NA) exceeded 3 μ relative to the group mean, this individual was considered to be unduly influencing the group mean as a result of blood contamination and was removed from the final analysis. For skeletal muscle CD4+ T-cell data, as a result of an unforeseen effect of the Dispase II enzyme on the CD4 receptor as reported previously (Abuzakouk *et al.* 1996), this outcome represents a total *n* of 10 (Young) and 5 (Old) for CD4+ T-cell results. Furthermore, because of the small tissue biopsy yields, insufficient sample was obtained in some individuals for flow cytometry [<250 mg (adipose tissue) and <35 mg (skeletal muscle) available]. This amounted to one missing adipose tissue sample from each group and two missing skeletal muscle samples for the Old group.

Biochemical analysis of adipose tissue culture and peripheral blood

Baseline blood samples were analysed for plasma glucose, HDL cholesterol, total cholesterol, triglycerides and non-esterified fatty acids (NEFA) using clinical chemistry spectrophotometer (RX Daytona, Randox Laboratories; County Antrim, Northern Island). Quantification of low-density lipoprotein (LDL)-cholesterol was achieved using the Friedwald equation (Friedewald *et al.* 1972). Insulin was measured using Insulin ELISA kits (Mercodia; Mercodia AB, Uppsala, Sweden). A further 24 biomarkers of inflammation, cytokines and adipokines were measured in fasted plasma and adipose cell culture supernatant using R-plex, U-plex and V-plex kits on a QuickPlex SQ120 (Mesoscale Diagnostics, LLC, Maryland, USA). A human leptin ELISA kit (Quantikine; Bio-Techno Ltd, Minneapolis, MN, USA) was used to assess *ex vivo* leptin release by adipose tissue.

Statistical analysis

Comparisons between Old and Young groups were made using two-way independent samples *t* tests where normally distributed, and Mann–Whitney *U* non-parametric equivalents where Shapiro–Wilks distribution tests were violated ($P > 0.05$). Meal tolerance test data were analysed by repeated measures, two-way ANOVA with Bonferroni adjustments. Serial measurements of glucose, insulin, triglycerides and NEFAs were converted into summary statistics to illustrate the net response of each parameter using

the trapezoid method for total area under the curve (Matthews *et al.* 1990). Homeostasis model assessment for insulin resistance (HOMA–IR) was estimated using the equation by Matthews *et al.* (1985): fasting glucose (mmol L^{-1}) × fasting insulin (mU L^{-1})/22.5. Adipocyte size distribution data were analysed by multiple *t* tests with Benjamini and Yekutieli FDR corrections applied. Descriptive data are presented as the mean ± SD, with the exception of DESeq2 outputs, which are presented as the mean ± SE as standard according to the analysis output provided by usegalaxy.org. Statistical analysis was performed using Prism, version 9.0.1 (GraphPad Software Inc., San Diego, CA, USA) and SPSS, version 22 (IBM Corp., Armonk, NY, USA). $P \leq 0.05$ was considered statistically significant.

Results

Participant characteristics

Table 1 outlines the characteristics of Young and Old groups. There were no significant differences between groups for PAL ($P = 0.347$), body mass ($P = 0.112$), body mass index ($P = 0.695$), systolic blood pressure ($P = 0.173$), HOMA-IR ($P = 0.178$), fasting HDL-cholesterol ($P = 0.291$), triglycerides ($P = 0.242$), glucose ($P = 0.590$), NEFA ($P = 0.925$) and insulin ($P = 0.160$) (Table 1). There were small but consistent differences between groups for measures of body composition, adipose distribution, and RMR in Young compared to Old. Although all participants were within pre-determined ranges for inclusion, spanning from 'normal' to very low 'overweight' categories, FMI was modestly higher in Old compared to Young ($P = 0.001$). The Old group also had higher total cholesterol ($P = 0.009$), LDL-cholesterol ($P = 0.003$) and diastolic blood pressure ($P = 0.009$) (Table 1). There was also an almost 2-fold significantly higher level of plasma carboxymethyl lysine residue abundance in the plasma of Old compared to Young ($P = 0.019$) (Table 1). Dietary intake was similar across groups (Table 1). There were no significant differences between groups for post-prandial plasma glucose ($F_{1,22} = 1.395$, $P = 0.250$), insulin ($F_{1,22} = 1.004$, $P = 0.327$), NEFAs ($F_{1,22} = 1.331$, $P = 0.261$) or triglycerides ($F_{1,22} = 0.985$, $P = 0.332$) in response to a mixed-macronutrient drink (Fig. 2).

Adipose tissue and skeletal muscle exhibit unique stromal cell landscapes with age

Both adipose tissue and skeletal muscle exhibited a significantly higher number of CD4+ ($P = 0.021$ and 0.005, respectively) and CD8+ T-cells ($P = 0.034$ and 0.004, respectively) per gram of tissue in Old compared

Table 1. Characteristics of young and old groups

	Young (n = 12)	Old (n = 12)	P
Age (years)	27 ± 4	66 ± 5	<0.001[a]
Height (m)	1.84 ± 0.06	1.77 ± 0.05	0.012[a]
Body mass (kg)	83.0 ± 9.0	77.9 ± 5.5	0.112[a]
Body mass index (kg m^{-2})	24.5 ± 1.4	24.8 ± 1.4	0.695[a]
Waist-hip ratio	0.88 ± 0.03	0.95 ± 0.04	<0.001[b]
Fat mass index (kg m^{-2})	4.8 ± 1.0	6.0 ± 0.9	0.001[b]
Total bone mineral content (kg) (DEXA)	3.3 ± 0.4	2.8 ± 0.3	0.002[a]
Fat-free mass (kg) (DEXA)	62.7 ± 7.4	55.6 ± 5.1	0.012[a]
Fat mass (kg) (DEXA)	16.1 ± 3.7	18.8 ± 2.7	0.020[b]
Estimated visceral adipose tissue mass (g) (DEXA)	360 ± 89	728 ± 202	<0.001[b]
Physical activity level	1.79 ± 0.12	1.73 ± 0.16	0.347[b]
Resting metabolic rate (kcal day^{-1})	1942 ± 234	1666 ± 237	0.009[a]
Carbohydrate intake (g kg^{-1} BM)	3.4 ± 0.9	3.9 ± 1.2	0.283[a]
Protein intake (g kg^{-1} BM)	1.6 ± 0.5	1.3 ± 0.3	0.084[a]
Fat intake (g kg^{-1} BM)	1.2 ± 0.4	1.4 ± 0.4	0.503[a]
Fibre intake (g kg^{-1} BM)	0.3 ± 0.1	0.4 ± 0.4	0.387[b]
Systolic blood pressure (mmHg)	124 ± 9	132 ± 18	0.173[a]
Diastolic blood pressure (mmHg)	80 ± 4	87 ± 7	0.009[b]
Total cholesterol (mmol L^{-1})	4.3 ± 0.9	5.4 ± 1.2	0.007[b]
HDL cholesterol (mmol L^{-1})	1.1 ± 0.3	1.2 ± 0.3	0.291[b]
LDL cholesterol (mmol L^{-1})	2.7 ± 0.5	3.7 ± 0.9	0.003[b]
Triglycerides (mmol L^{-1})	0.98 ± 0.56	1.17 ± 0.43	0.242[b]
Glucose (mmol L^{-1})	5.33 ± 0.32	5.42 ± 0.27	0.590[b]
NEFA (mmol L^{-1})	0.39 ± 0.24	0.40 ± 0.19	0.925[a]
Insulin (pmol L^{-1})	33.3 ± 15.9	36.7 ± 10.4	0.160[b]
HOMA-IR	1.33 ± 0.68	1.47 ± 0.41	0.178[b]
Plasma CML residues (AU μL^{-1} plasma)	5.87 ± 0.70	9.03 ± 1.03	0.019[a]

All measures (excluding dietary intake data) were taken following an overnight fast. Dietary intake data are representative of 3 days' (2 weekdays; 1 weekend day) recording. Plasma CML residues were measured by semi-quantitative immunoblotting. Data are presented as the mean ± SD.
[a] An independent-samples *t* test was performed.
[b] A Mann–Whitney *U* test was performed.
AU, arbitrary units; BM, body mass; CML, carboxymethyl lysine; HDL, high-density lipoprotein; HOMA-IR, homeostatic model of insulin resistance; LDL, low-density lipoprotein; NEFA, non-esterified fatty acids.

to Young (Fig. 3*A* and 3*B*). The number of CD4+ cells in peripheral blood was not impacted by age ($P = 0.368$), whereas CD8+ numbers were significantly lower ($P = 0.042$) in Old compared to Young (Fig. 3*C*).

Further analyses of CD4+ T-cell subsets showed that both central (CM) and effector memory cells (EM) (CD27+CD45RA− and CD27−CD45RA−, respectively) were significantly more abundant in Old compared to Young in both adipose and muscle ($P = 0.021$, 0.031, 0.021 and 0.031 for adipose tissue and skeletal muscle CD4+ CM and EM T-cells, respectively). By contrast, no differences were observed for the naïve (NA) and terminally differentiated effector memory cells (EMRA) (CD27+CD45RA+ and CD27−CD45RA+, respectively) ($P = 0.158$, 0.762, 0.768 and 0.313 for adipose tissue and skeletal muscle CD4+ NA and EMRA T-cells, respectively) (Fig. 3*D* and 3*E*). Similarly, for the CD8+

T-cell subpopulations, CM and EM cells were significantly elevated in Old compared to Young across both adipose ($P = 0.043$ and 0.002, respectively) and muscle ($P = 0.002$ and 0.002, respectively) (Fig. 3*G* and 3*H*), whereas only muscle exhibited a significantly greater number of CD8+ EMRA cells in Old compared to Young ($P = 0.047$) (Fig. 3*H*).

There was also double the number of macrophages per gram of skeletal muscle in Old compared to Young ($P = 0.002$) (Fig. 3*B*), whereas adipose tissue macrophage abundance was not different between groups ($P = 0.824$) (Fig. 3*A*). Macrophage surface expression of HLA-DR was not different between groups in either adipose tissue or skeletal muscle ($P = 0.124$ and 0.115, respectively) (Fig. 3*J* and 3*K*). Within the SSC–A^{high}CD14− granulocyte fraction, adipose tissue CD16− granulocytes were significantly more abundant in Old compared to Young
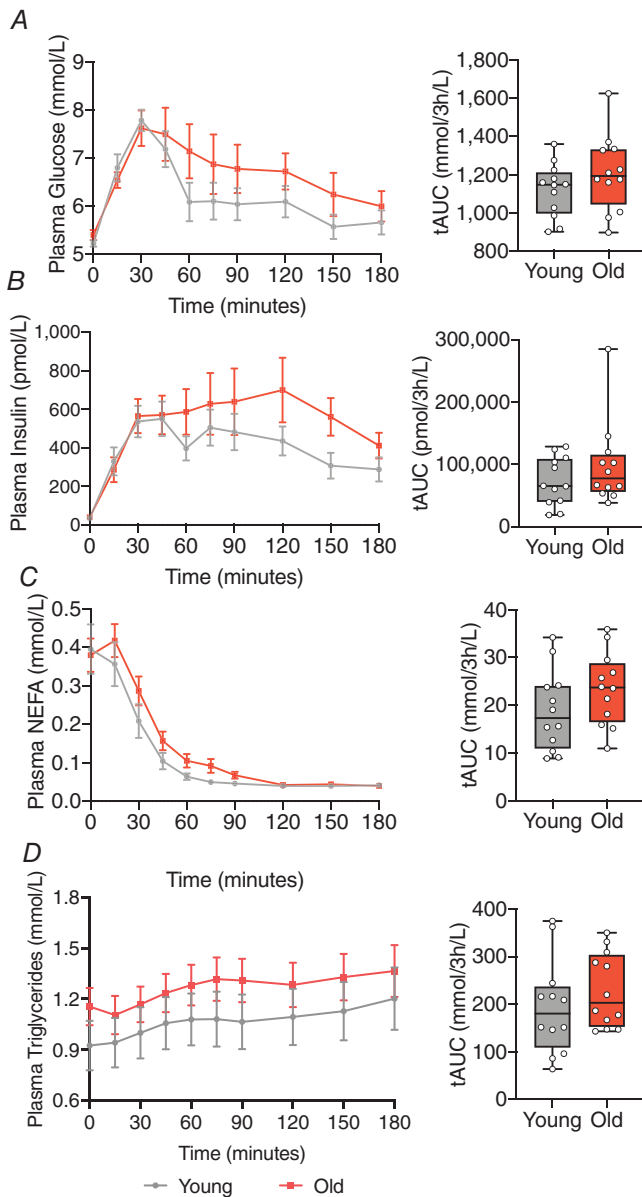
Figure 2. Plasma glucose, insulin, triglyceride and NEFA responses over 3 h following the consumption of a liquid mixed-meal, for Young and Old individuals
Temporal responses for (*A*) glucose, (*B*) insulin, (*C*) NEFAs and (*D*) triglycerides, alongside total area under the curve (tAUC) for each. Data represent *n* = 12 per group. Temporal data are presented as the mean ± SEM and tAUC data are presented as box-whisker min-to-max plots, where boxes represent median with 25th/75th quartiles, with whiskers from minimum to maximum values, with individual values overlaid. Continuous data were analysed using two-way repeated measures ANOVA with Bonferroni corrections. tAUC data were analysed using independent samples *t* tests or Mann–Whitney *U* tests where not normally distributed (Shapiro–Wilks, $P > 0.05$). [Colour figure can be viewed at wileyonlinelibrary.com]

($P = 0.034$) (Fig. 3*M*). Likewise, in skeletal muscle, both CD16+ neutrophils and CD16− granulocytes were significantly more abundant in Old compared to Young ($P = 0.001$ and 0.007, respectively) (Fig. 3*N*).

In blood, of the cell types measured, only total CD8+ T-cells and naïve CD8+ T-cell numbers were significantly reduced in Old compared to Young ($P = 0.032$ and 0.037, respectively) (Fig. 3*C* and 3*I*). However, peripheral blood naïve CD4+ and EMRA CD8+ T-cell HLA-DR expression as a marker of activation was significantly lower in the Old compared to Young group ($P = 0.024$ and 0.028, respectively) (Fig. 4*A* and 4*D*). Likewise, adipose tissue and skeletal muscle EMRA CD8+ T-cell HLA-DR expression, on a per-cell basis, was also significantly lower in the Old compared to Young groups ($P = 0.051$ and 0.038, respectively) (Fig. 4*B* and 4*F*).

In the non-haematopoietic portion of skeletal muscle and adipose tissue progenitor cells were quantified. Progenitor cell number (identified as CD45−CD31−CD34+ in adipose tissue and CD45−CD15+CD56− in skeletal muscle) was similar across groups (both $P > 0.999$) (Fig. 5*A* and 5*D*), although the expression of the adipocyte progenitor marker CD140a was significantly greater on a per-cell basis in Old muscle and adipose tissue ($P = 0.002$ and $P < 0.0001$, respectively) (Fig. 5*B* and 5*E*). The relative cell surface expression of CD140a was ∼10-fold higher in Old muscle compared to adipose tissue. Within skeletal muscle, CD45−CD56+ cells were also identified as a general marker of satellite cells, which were significantly more abundant within the Old group compared to Young ($P = 0.009$) (Fig. 5*C*). Likewise, CD45−CD31+CD34+ pan-endothelial cells were identified in the adipose tissue, but were similar across groups in number ($p = 0.112$) (Fig. 5*F*).

Analysis of the proportional breakdown of both adipose tissue and skeletal muscle SVFs is presented in Fig. 6*A* and 6*B*. These analyses revealed a significantly greater total CD45+ pool relative to CD45− in Old compared to Young adipose tissue ($P < 0.001$) (Fig. 6*A*). Furthermore, within the adipose tissue CD45+ portion, non-CD4+ and non-CD8+ CD3+ T-cells (i.e. double-negative T-cells) were significantly lower in Old compared to Young ($P = 0.016$), as was the proportional representation of CD206+ macrophages within the CD45+ pool ($P = 0.022$) (Fig. 6*A*). In the skeletal muscle SVF, the proportion of CD45+ cells (i.e. cell subtypes not phenotyped) was significantly smaller in Old compared to Young ($P = 0.048$) (Fig. 6*B*). A cumulative breakdown of absolute CD45+ cell counts is presented in Fig. 6*C*, representing cell counts from cell populations displayed as proportions in Fig. 6*A* and 6*B*. In both adipose tissue and skeletal muscle, total CD45+ cell counts were almost 3-fold higher in Old compared to Young ($P = 0.004$ and $P = 0.003$, respectively) (Fig. 6*C*).
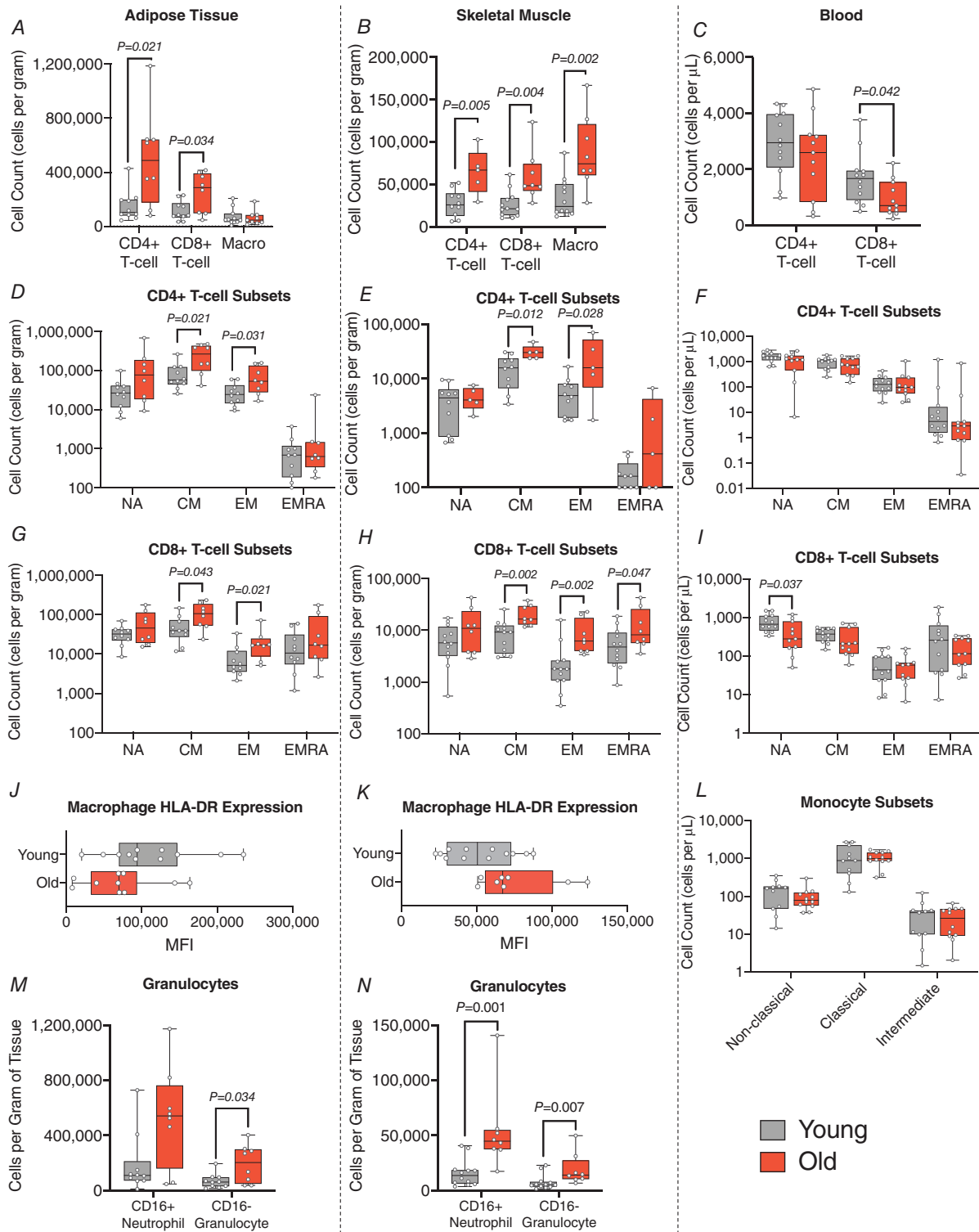
Figure 3. Adipose tissue, skeletal muscle, and peripheral blood T-cells, macrophages and monocytes in Young and Old individuals

A, adipose tissue CD4+ and CD8+ T-cells and CD206+ macrophages. Young (*n* = 10–11); Old (*n* = 8–9). *B*, skeletal muscle CD4+ and CD8+ T-cells and CD206+ macrophages. Young (*n* = 10–12); Old (*n* = 5–12). *C*, peripheral blood CD4+ and CD8+ T-cells. Young (*n* = 12); Old (*n* = 12). *D*, adipose tissue CD4+ T-cell subpopulations. Young (*n* = 10); Old (*n* = 8). *E*, skeletal muscle CD4+ T-cell subpopulations. Young (*n* = 9–10); Old (*n* = 5). *F*, peripheral blood CD4+ T-cell subpopulations. Young (*n* = 12); Old (*n* = 12). *G*, adipose tissue CD8+ T-cell subpopulations. Young (*n* = 10); Old (*n* = 8). *H*, skeletal muscle CD8+ T-cell subpopulations. Young (*n* = 12); Old (*n* = 8). *I*, peripheral blood CD8+ T-cell subpopulations. Young (*n* = 12); Old (*n* = 12). *J*, adipose tissue macrophage HLA-DR median

fluorescence intensity (MFI). Young ($n = 11$); Old ($n = 10$). K, skeletal muscle macrophage HLA-DR MFI. Young ($n = 12$); Old ($n = 9$). L, peripheral blood monocyte subpopulations. Young ($n = 11$); Old ($n = 12$). Cell counts represent absolute cell counts per gram of tissue. Boxes represent median with 25th/75th quartiles, with whiskers from minimum to maximum values, with individual values overlaid. Data were analysed using independent samples *t* tests or Mann–Whitney *U* tests where not normally distributed (Shapiro–Wilks $P > 0.05$). [Colour figure can be viewed at wileyonlinelibrary.com]

Adipose tissue exhibits a pro-inflammatory phenotype with ageing

There was a significantly greater secretion of IL-6, IL-17D, RANTES (Regulated upon Activation, Normal T Cell Expressed and Presumably Secreted), macrophage inflammatory protein (MIP)-3α, IL-8, interferon inducible protein-10, intercellular adhesion molecule (ICAM)-1, vascular cell adhesion molecule (VCAM)-1,
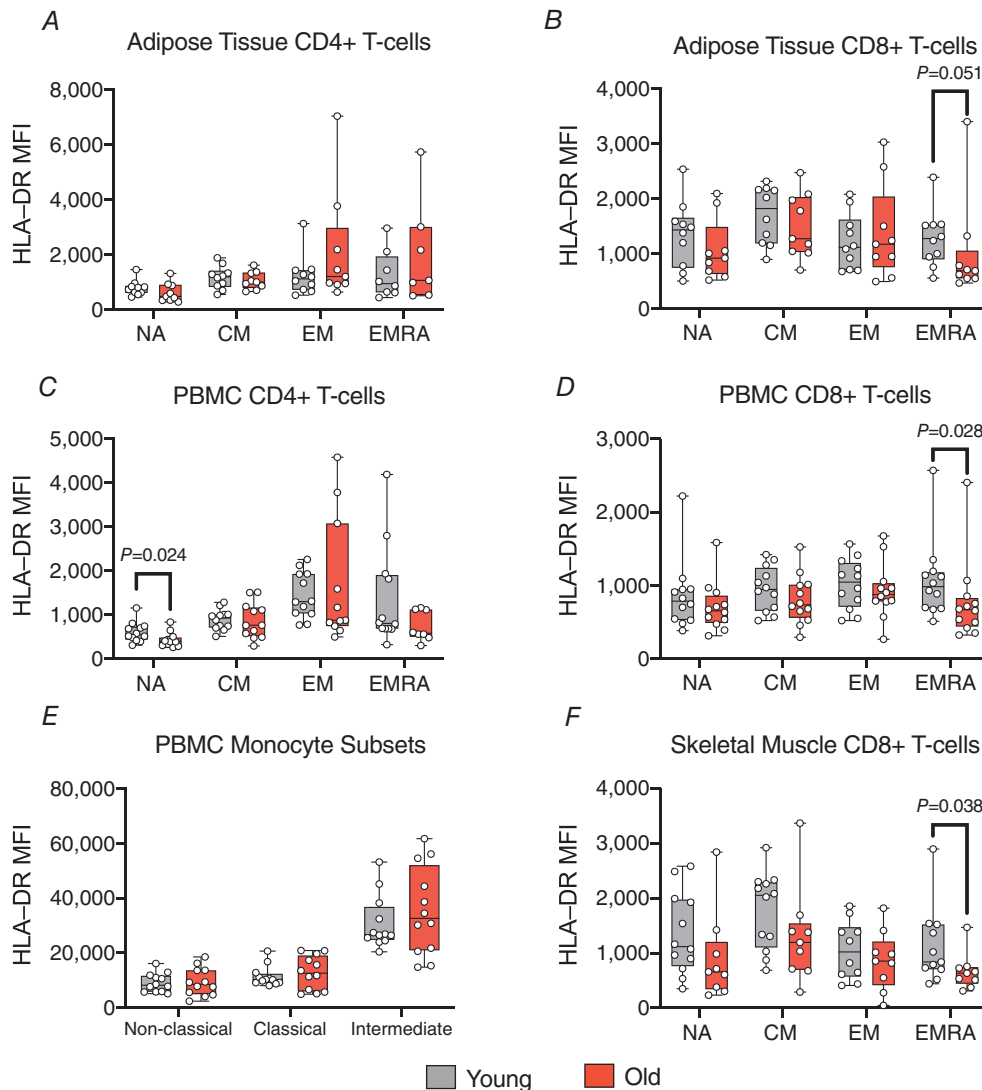

Figure 4. CD4+, CD8+ T-cell and monocyte subset HLA-DR expression across adipose tissue, skeletal muscle, and peripheral blood between Young and Old
A, adipose tissue CD4+ T-cell subset activation. Young ($n = 8$–10); Old ($n = 7$–9). *B*, adipose tissue CD8+ T-cell subset activation. Young ($n = 10$); Old ($n = 9$). *C*, PBMC CD4+ T-cell subset activation. Young ($n = 12$); Old ($n = 8$–12). *D*, PBMC CD8+ T-cell subset activation. Young ($n = 12$); Old ($n = 12$). *E*, PBMC monocyte subset activation. Young ($n = 12$); Old ($n = 12$). *F*, skeletal muscle CD8+ T-cell subset activation. Young ($n = 10$–12); Old ($n = 9$). Boxes represent median with 25th/75th quartiles, with whiskers from minimum to maximum values, with individual values overlaid. Data were analysed with independent samples *t* tests and Mann–Whitney *U* tests where not normally distributed (Shapiro–Wilks, $P > 0.05$). [Colour figure can be viewed at wileyonlinelibrary.com]

vascular endothelial growth factor (VEGF)-A, granzyme A, adipsin and resistin from *ex vivo* cultured Old adipose tissue explants compared to Young ($P = 0.002-0.052$) (Fig. 7*A*) indicative of a pro-inflammatory phenotype. Tumour necrosis factor (TNF)-α and inteferon (IFN)-γ were below the limits of detection in adipose tissue culture media. Plasma concentrations of IL-6, IL-17D, monocyte chemoattractant protein (MCP)-1, IL-8, VEGF-A, adipsin and adiponectin were significantly higher in Old compared to Young, whereas IL-4 was lower ($P \leq 0.0001-0.038$) (Fig. 7*B*).

Ageing impacts adipose tissue and skeletal muscle transcriptomes

Transcriptomic analyses revealed substantial differences in tissue transcriptomes in both adipose tissue and skeletal muscle between Young and Old with 463 and 913 differentially expressed genes (DEGs) between groups, respectively. In both tissues, there were also considerably more up-regulated DEGs than those down-regulated with age. There were 142 and 321 significantly down/up-regulated transcripts between Young and Old adipose tissue, respectively (Fig. 8*A*
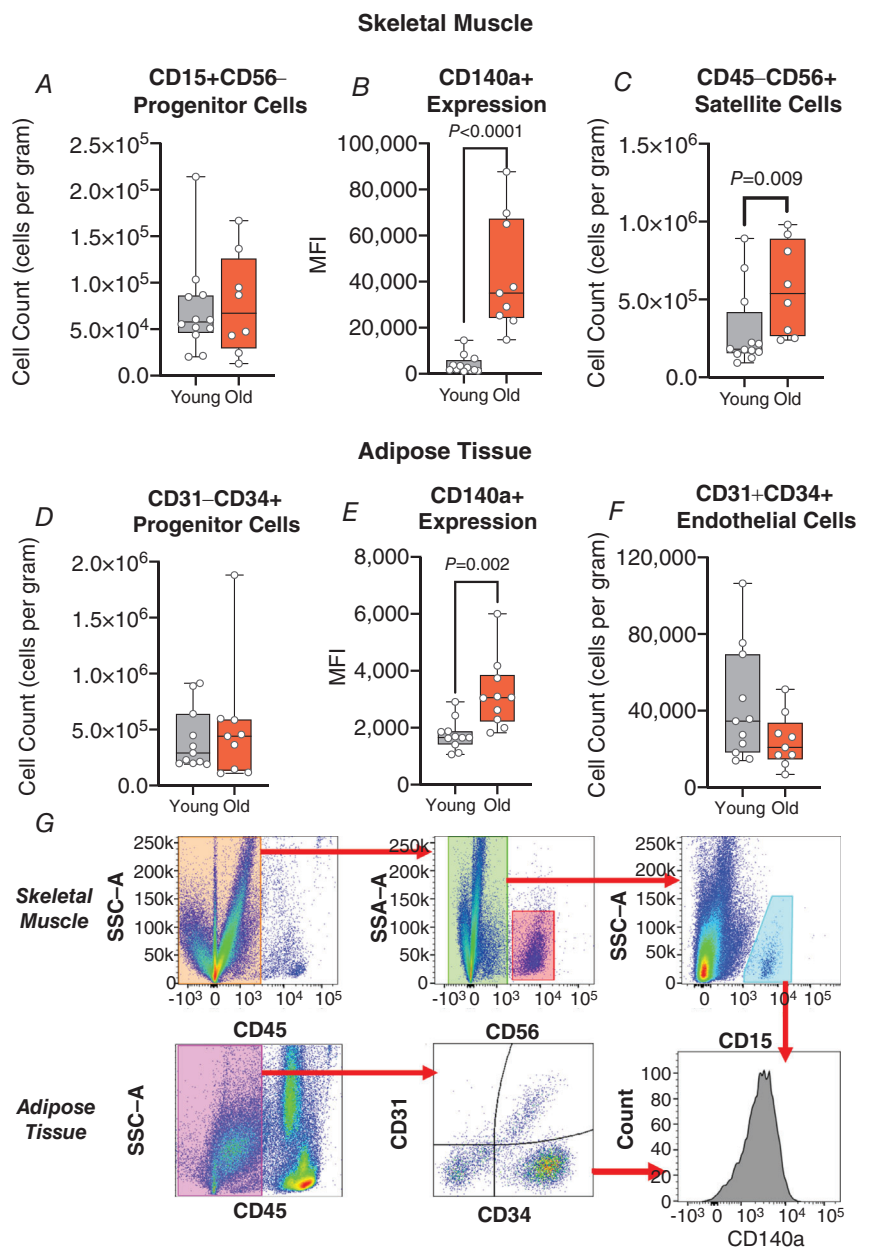

Figure 5. Skeletal muscle and adipose tissue non-haematopoietic cell quantification in young and old individuals

A, skeletal muscle CD15+CD56− progenitor cells. Young ($n = 12$); Old ($n = 8$). *B*, skeletal muscle CD31−CD34+ progenitor cell CD140a MFI. Young ($n = 12$); Old ($n = 8$). *C*, skeletal muscle CD56+ satellite cells. Young ($n = 12$); Old ($n = 8$). *D*, adipose tissue CD31−CD34+ progenitor cells. Young ($n = 11$); Old ($n = 9$). *E*, adipose tissue CD31−CD34+ progenitor cell CD140a MFI. Young ($n = 11$); Old ($n = 10$). *F*, adipose tissue CD31+CD34+ endothelial cells. Young ($n = 11$); Old ($n = 10$). *G*, representative gating profiles for skeletal muscle and adipose tissue adipocyte progenitors, adipose tissue endothelial cells and skeletal muscle satellite cells (singlets and all viable events were gated prior to SSC-A *vs.* CD45 gating, detailed in Fig. 1*I*–1*K*). Cell counts represent absolute cell counts per gram of tissue. Boxes represent median with 25th/75th quartiles, with whiskers from minimum to maximum values, with individual values overlaid. Data were analysed using independent samples *t* tests or Mann–Whitney *U* tests where not normally distributed (Shapiro–Wilks, $P > 0.05$). [Colour figure can be viewed at wileyonlinelibrary.com]

and 8*B*) and 346 and 567 significantly down/up-regulated transcripts in skeletal muscle (Fig. 8*C* and 8*D*). The 10 most up/down-regulated transcripts between Young and Old in adipose and muscle are presented in Fig. 8*E* and 8*F*. To identify whether ageing was associated with any shared transcriptomic differences, up- and down-regulated transcripts in adipose tissue and skeletal muscle were compared (Fig. 8*G*). Nine transcripts were found to be up-regulated in both adipose tissue and skeletal muscle in Old relative to Young, whereas eight transcripts were found to be down-regulated in both adipose tissue and skeletal muscle in Old relative to Young (Table 2).
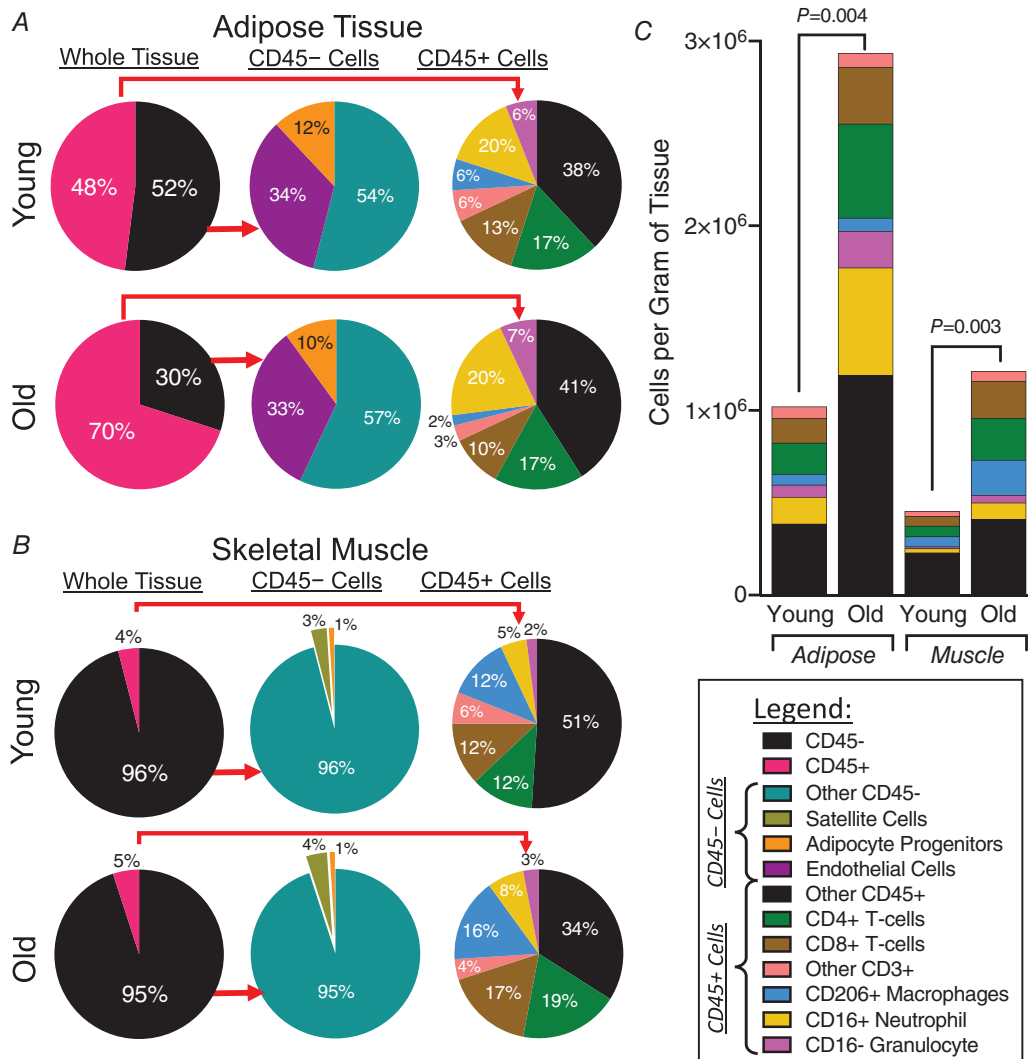

Figure 6. Adipose tissue and skeletal muscle SVF proportional and cell count breakdown between Young and Old individuals

A, proportional breakdown of adipose tissue for Young (top set of three wheels) and Old (bottom set of three wheels). Red lines indicate the subfractionation, and taking forward of either CD45− or CD45+ fractions. Pie charts are laid out as: left wheels = CD45+/− SVF split; middle wheels = CD45− cells proportional breakdown; right wheels = CD45+ cells proportional breakdown. Cell type proportional representations (%) are displayed with/within respective segments. Young (*n* = 10); Old (*n* = 8). *B*, proportional breakdown of skeletal muscle for Young (top set of three wheels) and Old (bottom set of three wheels). Red lines indicate the subfractionation, and taking forward of either CD45− or CD45+ fractions. Pie charts are laid out as: left wheels = CD45+/− SVF split; middle wheels = CD45− cells proportional breakdown; right wheels = CD45+ cells proportional breakdown. Cell type proportional representations (%) are displayed with/within respective segments. Young (*n* = 8); Old (*n* = 4). *C*, cumulative cell counts per gram of tissue for the CD45+ fraction of adipose tissue and skeletal muscle, between Young and Old individuals. Young [*n* = 10 (adipose tissue); *n* = 8 (muscle)]; Old [*n* = 8 (adipose tissue); *n* = 4 (muscle)]. All data represent respective group means. Data were analysed using independent samples *t* tests or Mann–Whitney *U* tests where not normally distributed (Shapiro–Wilks, *P* > 0.05). [Colour figure can be viewed at wileyonlinelibrary.com]

Consequently, <2 % of all DEGs in adipose tissue and skeletal muscle shared their response across tissues, with age.

All of the significantly ($q < 0.05$) up or down-regulated transcripts revealed by DESeq2 analyses (142 and 321 transcripts in adipose tissue, respectively, and 346 and 567 transcripts in skeletal muscle, respectively), were taken forward for GO analysis to further explore the gene networks associated with all DEGs between Young and Old in both adipose tissue and muscle. Over half of the up-regulated GO-biological processes (BPs) (13/25) in adipose tissue were associated with pro-inflammatory processes (Fig. 8*H*, purple), whereas skeletal muscle did not exhibit any GO-BPs related to pro-inflammatory

processes. In adipose tissue, GO-BPs associated with up-regulated DEGs between Young and Old were related to both innate and acquired immune processes, and the mounting of inflammatory responses (i.e. T-cell proliferation, B-cell proliferation, immune response, neutrophil chemotaxis, and innate and inflammatory immune responses, etc.). Moreover, there were pathways up-regulated in adipose tissue associated with the recruitment of immune cells, including chemotaxis, cell adhesion and integrin-mediated signalling pathways. These observations were also supported by similar trends in KEGG, GO-molecular function and GO-cellular compartment analyses in adipose tissue and skeletal muscle (data not shown).
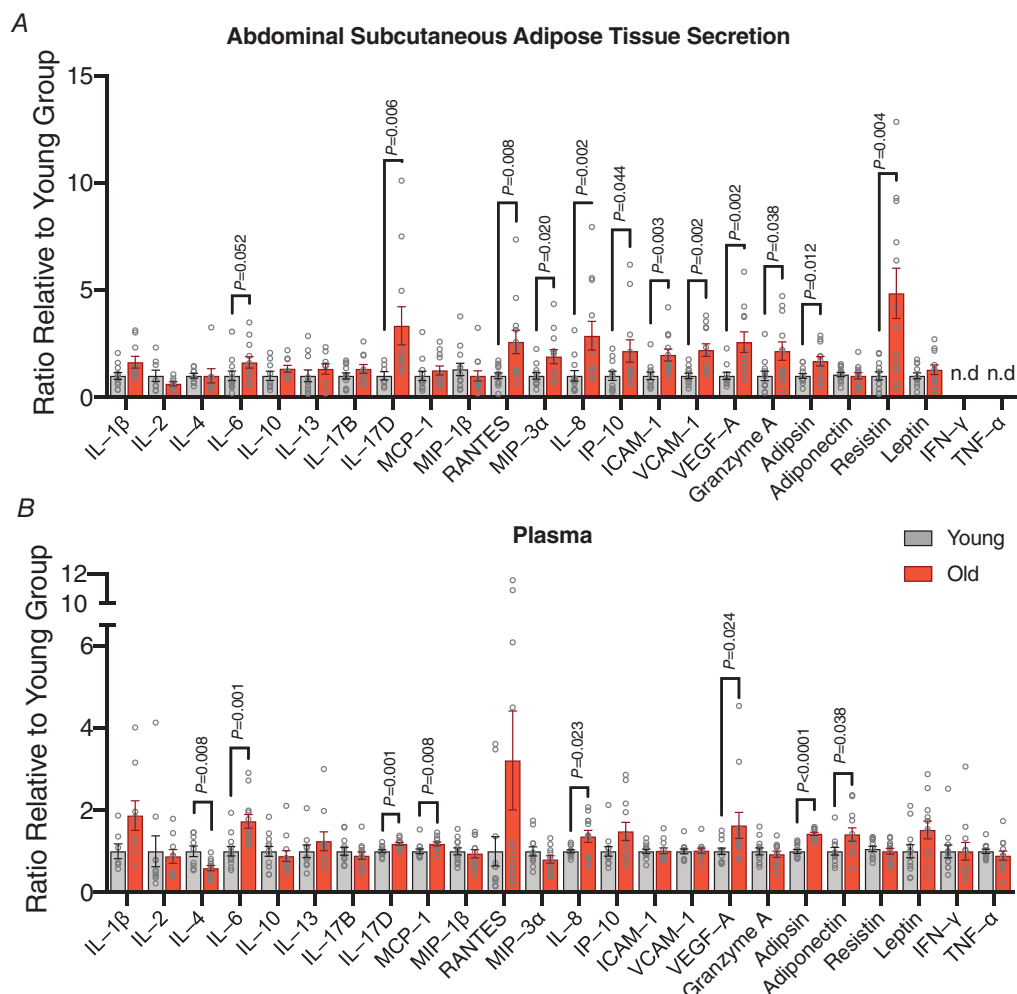

Figure 7. Adipose tissue-secretion and plasma protein profile in Young and Old individuals

A, abdominal subcutaneous adipose tissue secretion profile during 3 h of *ex vivo* culture. Data represent the ratio of protein secretion, relative to the Young group average from three or four adipose tissue technical replicates per participant, and represent protein secretion of adipose tissue cultured at a ratio of 50 mg of tissue per mL of culture media. Young ($n = 7$–12); Old ($n = 8$–12). *B*, plasma protein profile. All data are expressed as a ratio relative to the Young group mean for each respective protein. Young ($n = 7$–12); Old ($n = 9$–12). Data are presented as the mean ± SEM, with individual data points overlaid. n.d., not detected. Data were analysed using independent samples *t* tests or Mann–Whitney *U* tests where not normally distributed (Shapiro–Wilks, $P > 0.05$). [Colour figure can be viewed at wileyonlinelibrary.com]
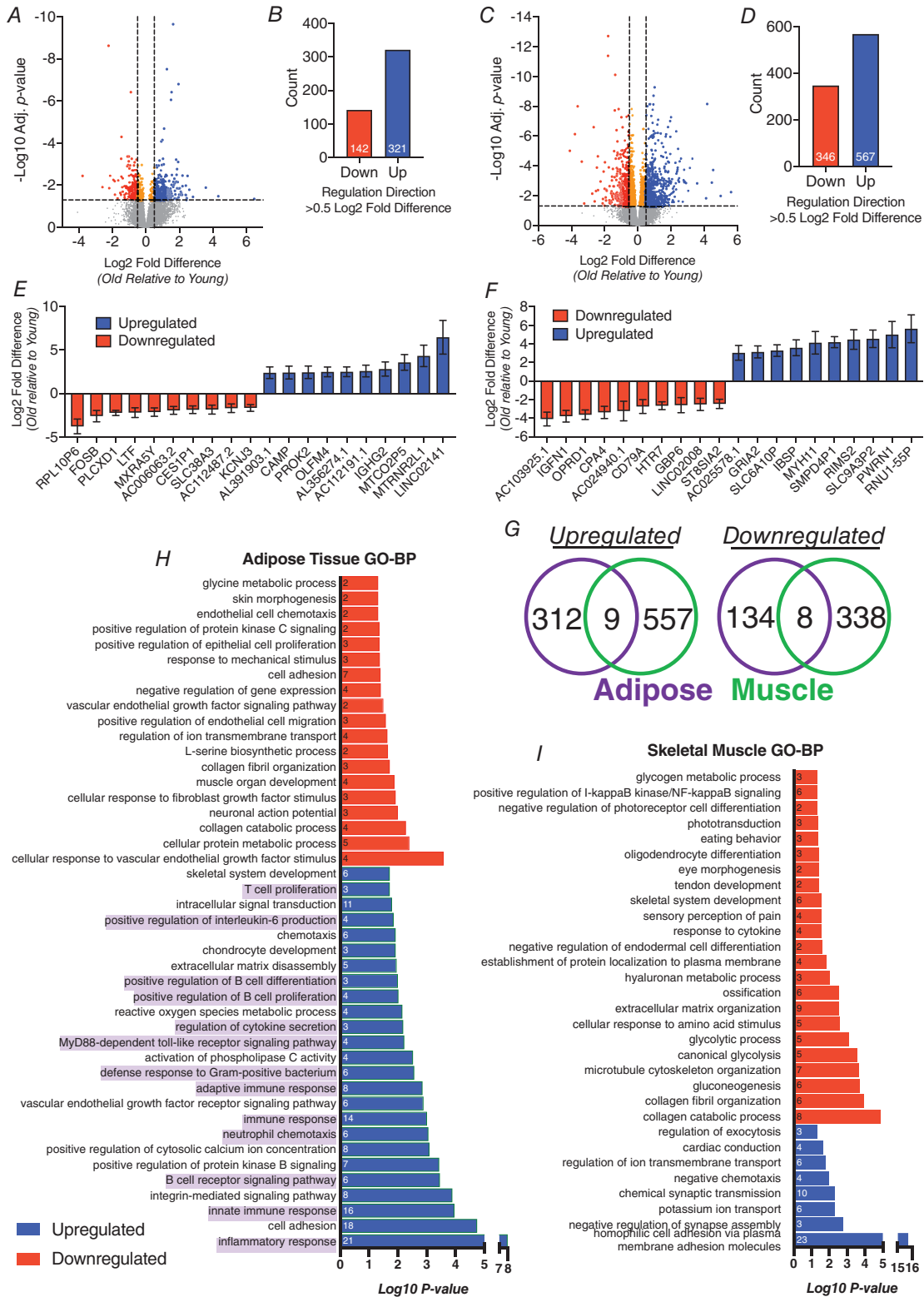
Figure 8. Adipose tissue and skeletal muscle transcriptional differences between Young and Old individuals (*n* = 11 and 12 per group for adipose tissue and skeletal muscle, respectively)

A, volcano plot of transcripts by log2 fold difference against DESeq2-adjusted *P* values (referred to as *q* values) in adipose tissue. Red dots, significantly down-regulated; green dots, significantly up-regulated; orange dots, significantly differentially expressed genes (DEGs) within 0.5 log2 fold difference; grey dots, non-DEGs. Significance was set at *q* < 0.05 (DESeq2). *B*, quantification of DEGs from (*A*). Significance was set at *q* < 0.05 (DESeq2). *C*,

volcano plot of transcripts by log2 fold difference against DESeq2 adjusted *P* values in skeletal muscle. Red dots, significantly down-regulated; green dots, significantly up-regulated; orange dots, significantly DEGs within 0.5 log2 fold difference; grey dots, non-DEGs. Significance was set at $q < 0.05$ (DESeq2). D, quantification of DEGs from (C). Significance was set at $q < 0.05$ (DESeq2). E, top-10 significantly up/down-regulated transcripts by magnitude of log2 fold difference between groups in adipose tissue. Data are presented as the mean ± SEM. Significance was set at $q < 0.05$ (DESeq2). F, top-10 significantly up/down-regulated transcripts by magnitude of log2 fold difference between groups in skeletal muscle. Data are presented as the mean ± SEM. Significance was set at $q < 0.05$ (DESeq2). G, Venn diagram of up- and down-regulated transcripts across adipose tissue and skeletal muscle to identify shared up/down-regulated transcripts across tissues. H, top-25 up/down-regulated gene ontology-biological processes (GO-BPs) in adipose tissue. Purple highlight represents a GO-BP related to inflammation. I, top-25 up/down-regulated GO-BPs in skeletal muscle. A and C, dotted lines indicate significance threshold ($q < 0.05$, horizontal) and >0.5 log2 fold difference (>0.5/< −0.5 log2 fold change, vertical). The specific number of hits within a given pathway from the DEGs put into the analyses are presented within each respective bar. A minimum threshold of two genes within a given pathway was set for consideration. Significance was set at $P < 0.05$ (EASE score) using DAVID 6.8. *P* values are presented as log10 values. [Colour figure can be viewed at wileyonlinelibrary.com]

Table 2. Shared up- and down-regulated transcripts across adipose tissue and skeletal muscle

	Adipose tissue		Skeletal muscle	
	Log2 Fold Difference (Young *vs* Old)	*P*	Log2 Fold Difference (Young *vs* Old)	*P*
Gene name	**Shared up-regulated**			
AC021517.1	0.80 ± 0.22	0.031	1.88 ± 0.42	<0.001
AC104564.5	0.77 ± 0.18	0.006	0.52 ± 0.15	0.017
AL157396.1	1.96 ± 0.50	0.014	1.83 ± 0.35	<0.001
CYP1B1-AS1	0.66 ± 0.13	0.001	0.95 ± 0.26	0.009
GCNT2	0.92 ± 0.16	<0.001	1.42 ± 0.39	0.009
LGI1	1.58 ± 0.45	0.032	1.34 ± 0.31	0.001
LINC02028	0.93 ± 0.23	0.012	0.84 ± 0.24	0.013
LINC02432	1.44 ± 0.41	0.033	1.68 ± 0.40	0.001
ZNF385B	1.53 ± 0.23	<0.001	0.71 ± 0.22	0.026
Gene name	**Shared down-regulated**			
COL1A1	−0.97 ± 0.26	0.021	−1.99 ± 0.50	0.003
COL1A2	−0.55 ± 0.16	0.039	−0.97 ± 0.28	0.014
DMRT2	−0.70 ± 0.16	0.005	−1.07 ± 0.29	0.007
FAM222A	−1.00 ± 0.22	0.003	−0.72 ± 0.22	0.021
PGK1P2	−1.26 ± 0.36	0.037	−0.95 ± 0.29	0.022
RET	−1.47 ± 0.28	<0.001	−0.52 ± 0.14	0.009
SLC25A25	−0.62 ± 0.18	0.041	−0.56 ± 0.15	0.006
SLC9C1	−1.25 ± 0.37	0.046	−1.04 ± 0.25	0.002

Data represent the difference in expression for each transcript from Old relative to Young individuals across adipose tissue ($n = 11$ per group) and skeletal muscle ($n = 12$ per group). Data represent the shared up- and down-regulated transcripts between groups for adipose tissue and skeletal muscle presented in Fig. 8*G*. Transcripts are ranked in alphabetical order. Zero represents no difference between groups. Data were analysed using DESeq2 and are presented as the mean ± SE. Adjusted *P* values were produced by DESeq2

The content of insulin signalling proteins (but not transcripts) is lower in adipose tissue with age

To assess the potential metabolic dysregulation occurring with ageing, we measured the protein expression of major components of the insulin signalling pathway leading to increased glucose uptake in adipose tissue and skeletal muscle. In adipose tissue from participants in the Old group, InsRβ, AS160 and GLUT4 protein levels were ∼0.5-fold lower than in the Young group ($P = 0.04$, 0.041 and 0.002, respectively) (Fig. 9*C*). A similar difference was also apparent for these three proteins in isolated adipocytes ($P = 0.022$, 0.029 and 0.018, respectively) (Fig. 9*E*). There were no statistically significant differences between groups within skeletal muscle for any of the insulin signalling proteins measured by immunoblotting ($P = 0.677$, 0.565, 0.401 and 0557 for InsR(β), Akt2, AS160 and GLUT4, respectively). For
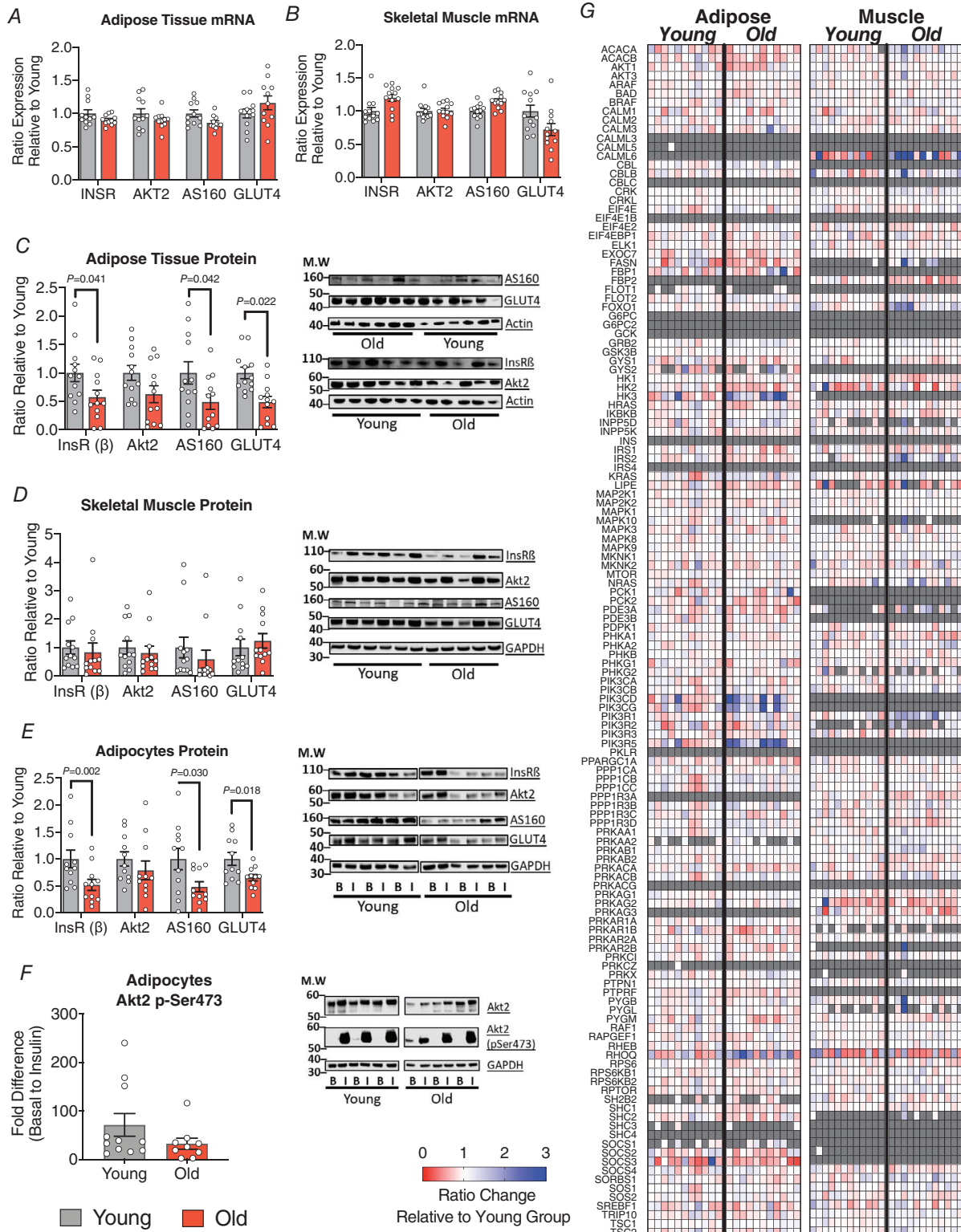
Figure 9. Adipose tissue and skeletal muscle insulin signalling gene expression, and adipose tissue, skeletal muscle and adipocyte protein expression in Young and Old individuals

A, adipose tissue mRNA expression for a range of targeted insulin signalling molecules extracted from transcriptomics analysis. Young (*n* = 11); Old (*n* = 11). *B*, skeletal muscle mRNA expression for a range of targeted insulin signalling molecules extracted from transcriptomics analysis. Young (*n* = 12); Old (*n* = 12). *C*, adipose tissue

protein expression for a range of targeted insulin signalling molecules. Young ($n = 12$); Old ($n = 12$). *D*, skeletal muscle protein expression for a range of targeted insulin signalling molecules. Young ($n = 12$); Old ($n = 12$). *E*, adipocyte protein expression for a range of targeted insulin signalling molecules. Young ($n = 11$); Old ($n = 11$). *F*, Akt phosphorylation in isolated adipocytes represented as fold difference in Akt2 phosphorylation at Ser473 from unstimulated (*B*) to stimulated (*I*) (100 nM insulin for 30 min, *ex vivo*) conditions. Representative blots are presented to the right of each respective graph. *G*, heat map of expression levels for mRNA transcripts within the KEGG insulin signalling pathway between Young and Old individuals in adipose tissue (left) and skeletal muscle (right), excluding those presented separately in (*A*) and (*B*). Data represent each individuals' expression level as a ratio relative to the Young group mean, for each respective transcript. Grey indicates that values fell below detectable limits. Data for (*A*) to (*E*) are displayed as a ratio of the Young group mean for each respective molecule, presented as the mean ± SEM, with individual data points overlaid. Data in (*A*), (*B*) and (*G*) were analysed by multiple *t* tests with Benjamini and Yekutieli FDR corrections applied. Data in (*C*) to (*F*) were analysed using independent samples *t* tests or Mann–Whitney *U* tests where not normally distributed (Shapiro–Wilks, $P > 0.05$). [Colour figure can be viewed at wileyonlinelibrary.com]

the purpose of direct comparison, all transcripts from the insulin signalling KEGG pathway were extracted from transcriptomics analyses in both tissues and were re-analysed using multiple unpaired *t* tests with Benjamini and Yekutieli FDR corrections applied. Of these extracted transcripts, *INSR*, *AKT2*, *TBC1D4* (AS160) and *SLC2A4* (GLUT4) are presented in Fig. 9*A* and 9*B* to facilitate direct comparison with their respective proteins measured by immunoblotting, with the remaining transcripts within the KEGG pathway presented in Fig. 9*G*. No statistically significant differences between groups were identified for any of the mRNA transcripts in adipose tissue or skeletal muscle (Fig. 9*A*, 9*B* and 9*G*). There were also no differences between Young and Old adipocytes for Akt2 phosphorylation at serine 473 in response to a supra-physiological *ex vivo* dose (100 nM) of insulin ($P = 0.201$) (Fig. 9*F*).

The abundance of large adipocytes is elevated with ageing

There were no differences between each decade diameter range between Young and Old ($P = 0.955\text{--}0.999$) (Fig. 10*A*). However, the proportion of adipocytes over 100 μm (hypertrophic adipocytes) was significantly higher in Old compared to Young ($P = 0.009$) (Fig. 10*B*) and the median adipocyte diameter was significantly greater [median (25th$-$75th percentile) $=$ 45.3 (34.8$-$56.8) *vs.* 41.2 (31.3$-$54.6) for Old *vs.* Young, respectively] ($P < 0.0001$) (Fig. 10*C*).

Discussion

This is the first study to examine the impact of biological ageing on adipose tissue in humans. We also compared
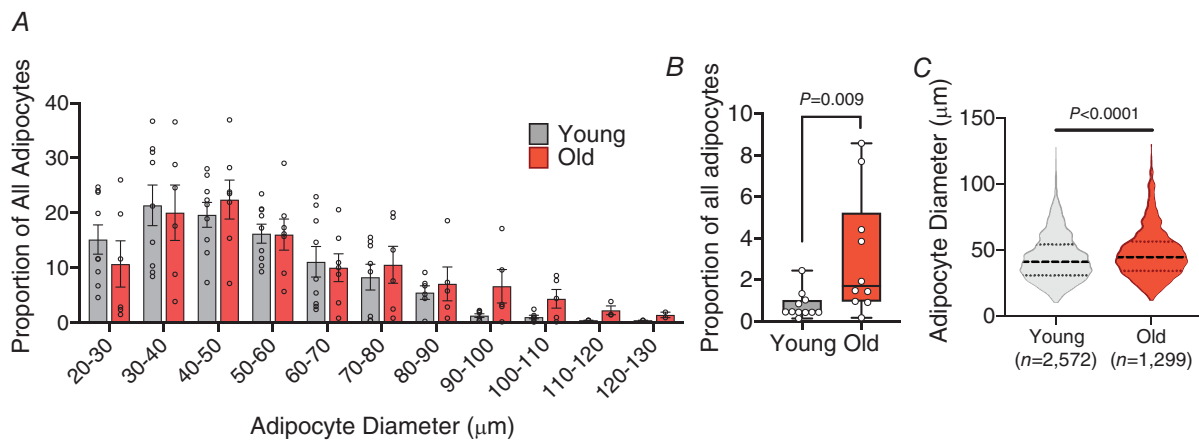

Figure 10. Adipocyte diameter distribution between Young and Old individuals
A, adipocyte size distribution between 20 and 130 μm, split by intervals of 10 μm. Bars represent the mean proportion a given range of adipocyte diameter (μm) represents within all measured adipocytes for each participant (minimum of 50 measures per individual), presented as the mean ± SEM with individual data points overlaid. Data were analysed by multiple *t* tests with Bejamini and Yekutieli FDR corrections applied. *B*, proportional representation of adipocytes ≥100 μm relative to all measured adipocytes. Boxes represent median with 25th/75th quartiles, with whiskers from minimum to maximum values. *C*, violin plot of adipocyte size distribution for all measured cells within each groups. Dark dashed lines represent group medians, with light dotted lines representing quartiles. *N*, the number under each group label represents the total number of adipocytes measured for each group. Data were analysed using independent samples *t* tests or Mann–Whitney *U* tests where not normally distributed (Shapiro–Wilks, $P > 0.05$). Young ($n = 9$); Old ($n = 7$). [Colour figure can be viewed at wileyonlinelibrary.com]

the effects of biological ageing on adipose tissue to those in skeletal muscle and blood from the same individuals. A key aspect to the current study design is that all participants were physically active and did not have excess adiposity, enabling better assessment of the impact of ageing *per se*. We demonstrate that ageing is associated with a substantial accumulation of T-cells in both adipose tissue and skeletal muscle, as well as an accumulation of macrophages in skeletal muscle, but not adipose tissue. This T-cell expansion primarily affected central memory and effector memory CD4+ and CD8+ T-cells in both tissues. Adipose tissue in older people also exhibited a pro-inflammatory, leukocyte-recruiting secretory phenotype and lower insulin signalling protein content. In skeletal muscle, but not adipose tissue, a greater abundance of macrophages was observed in older adults. Conversely, there was only modest systemic inflammation and metabolic impairment with ageing, suggesting that these tissue-specific observations may represent early manifestations of age-associated inflammation and metabolic deterioration.

In the present study, adipose tissue from healthy older adults contained around 2-fold more CD4+ and CD8+ T-cells, per gram of tissue compared to younger adults, primarily driven by greater numbers of central and effector memory cells. This is the first study to examine T-cells in paired adipose tissue and skeletal muscle samples from young and older humans, although similar observations have been reported in aged murine adipose tissue (Wu *et al.* 2007a; Lumeng *et al.* 2011). In mice, the age-associated accumulation of T-cells in adipose tissue leads to the production of IL-6, MCP-1 and TNF-α (Lumeng *et al.* 2011). Transcriptomic analysis in the present study also identified an enrichment of innate and acquired immune cell activation signalling pathways, pro-inflammatory signalling cascades, and pathways involved in the recruitment and trans-endothelial migration of immune cells into adipose tissue in older adults. However, we were unable to confirm by the surface expression of HLA-DR on CD4+ and CD8+ T-cells across the tissues and blood that there was a discernible change in their activation status. Although HLA-DR is a known marker of late-stage T-cell activation, other markers of activation such as CD69, major histocompatibility complex or CD38, or intracellular cytokine expression, might have been more specific to the form of activation T-cells undergo within aged adipose tissue (Ahnstedt *et al.* 2018). Future work should investigate whether adipose tissue lymphocytes are activated with ageing and, if so, which specific form of activation this represents. Whether adipose tissue lymphocyte accumulation is the primary factor explaining age-associated adipose tissue inflammation, as was suggested in mice (Lumeng *et al.* 2011), remains to be determined in humans. However, the present study

suggests T-cell accumulation in aged adipose tissue is a potential hallmark of age-associated adipose tissue dysfunction.

Some mechanisms by which T-cells enter adipose tissue have been established in the context of obesity. In obesity, it has been demonstrated that CCL20/CCR6 and CCR5/CCL5 interactions between adipocytes and T-cells drive adipose tissue T-cell accumulation (Wu *et al.* 2007b; Kintscher *et al.* 2008; Duffaut *et al.* 2009). In the present study, CCL5 (RANTES) and CCL20 (MIP-3α) were secreted at higher rates from adipose tissue from older participants when cultured *ex vivo*. Similarly, a significantly greater release of ICAM-1 and VCAM-1 from adipose tissue from older adults may also play a role in promoting lymphocyte infiltration, given the role of these adhesion molecules in T-cell tethering and transmigration (Steffen *et al.* 1994; Yang *et al.* 2005). Pathway analysis of transcriptomic data in the present study provides further support for this hypothesis. For example, networks linking the selective up-regulation of ICAM-1 and VCAM-1 expression by endothelial cells, which facilitate leukocyte migration into adipose tissue in response to resistin were up-regulated in the adipose tissue from older, compared to younger adults. These results corroborate the *ex vivo* tissue culture data that identified elevated ICAM-1, VCAM-1 and resistin release by adipose tissue from older individuals. It is also possible that heightened IL-17D secretion with ageing may also play a role in the observed immunological differences reported in adipose tissue between groups. IL-17D is preferentially expressed in adipose tissue and plays a role in chemokine induction, local immune responses and lymphocyte proliferation (Starnes *et al.* 2002), all of which were present in adipose tissue from older participants. Whether an orchestrated release of chemokines from adipose tissue occurs with ageing, or whether these observations are the result of tissue dysfunction, remains unknown.

Interestingly, however, there was no difference in *ex vivo* IL-2 release, which drives T-cell proliferation, in adipose tissue from older individuals, potentially suggesting that *in vivo* or *in situ* expansion of T-cells may not explain the observed increased T-cell abundance in adipose tissue from older individuals. The accumulation of T-cells in adipose may drive local inflammation, although it is also possible adipose tissue acts as a secondary lymphoid organ for the storage of memory T-cells following infections (Han *et al.* 2017). In this scenario, four or five decades of additional infections may explain the increased memory T-cell abundance in adipose tissue from older individuals in the present study. Thus, the significance of memory T-cell accumulation in adipose tissue is not yet fully clear and, although the adipose tissue may reflect a potential reservoir for immune cells, the accumulation of these cells post-infection may, over time, develop a

pro-inflammatory immune profile within the adipose tissue that is not necessarily beneficial to its function.

In the present study, there was no difference in adipose tissue macrophage content between groups. In the single available human study (Ortega Martinez de Victoria *et al.* 2009), there was a modest decline in adipose tissue macrophages as a proportion of the tissue SVF by 45 years of age. Despite this reported decline, macrophages adopted a pro-inflammatory gene expression profile, including plasminogen activator inhibitor 1 and CD11c (Ortega Martinez de Victoria *et al.* 2009). In aged mice, a similar reduction in CD206+ macrophage proportions has been shown (Wu *et al.* 2007a; Lumeng *et al.* 2011). Although we observed a decline in macrophage proportion within the CD45+ compartment of the SVF, we did not show a difference in absolute cell counts between groups. Future work should characterize the precise phenotype of tissue-resident macrophages in human adipose tissue of older adults given the potential heterogeneity of adipose tissue macrophages (Korf *et al.* 2019). Nonetheless, the present data indicate that age-associated adipose tissue dysfunction (in the absence of excess adiposity) may not be driven by classical (obesity-like) accumulation of macrophages.

Similar to adipose tissue, there was a substantial accumulation of central memory and effector memory CD4+ and CD8+ T-cells in muscle from older individuals. Both CD4+ and CD8+ T-cells are important effectors in the early reparative responses to muscle injury (Tidball, 2017), whereas chronically elevated CD4+ and CD8+ T-cell numbers within skeletal muscle has been associated with persistent muscle inflammation (Villalta *et al.* 2014). Furthermore, long-term exposure of skeletal muscle to the cytotoxic actions of T-cells has also been found in myopathies (Sugiura *et al.* 1999). Thus, T-cell accumulation in muscle with ageing might be implicated in the loss of muscle mass with age as a result of their propagation of a pro-inflammatory tissue microenvironment. Macrophages also have a fundamental role in the reparative process in response to muscle damage, facilitating the clear-up of injured tissue (Tidball, 2017). Macrophage accumulation in skeletal muscle from older individuals may reflect a normal response to the gradual loss of muscle mass that occurs with age (Delmonico *et al.* 2009; Barberi *et al.* 2013). Therefore, it could be speculated that the higher CD4+ and CD8+ T-cell counts in skeletal muscle from older individuals, as well as higher macrophages, may contribute to the development of sarcopenia in older adults, even when physical activity is maintained.

Substantially greater numbers of granulocytes were also apparent in both adipose tissue and muscle of the older compared to younger group. Granulocytes were also examined for their expression of CD16 (Gustafson *et al.* 2015). Our own observations in obese human adipose tissue shows that 95−96% of CD16+ granulocytes express the neutrophil marker CD66b, whereas ∼50% of CD16− granulocytes express the eosinophil-specific marker siglec-8 (W.V.Trim and L.Lynch, unpublished data). In adipose tissue, neutrophils promote inflammation and metabolic deterioration in the context of obesity (Talukdar *et al.* 2012; Watanabe *et al.* 2019), whereas eosinophils promote an anti-inflammatory microenvironment (Lee *et al.* 2018; Knights *et al.* 2020). We have shown that CD16− granulocytes in adipose tissue are more abundant in the older compared to younger group. Brigger *et al.* (2020) recently found that eosinophils are substantially reduced and their anti-inflammatory capabilities impaired in aged murine adipose tissue. Therefore, the considerable increase in CD16− granulocyte cells (which contains eosinophils) with age in the present study, in contrast to that reported in mice, suggests that this is a topic warranting further study in humans. We also show a non-statistically significant higher neutrophil count in adipose tissue from older participants compared to the young group, which RNA-sequencing analysis supports (i.e. an enrichment for neutrophil chemotaxis signalling transcripts according to GO-BP classification).

In skeletal muscle, we also show significantly increased numbers of CD16+ and CD16− granulocytes. Within skeletal muscle, neutrophils and eosinophils contribute to fibre repair, whereas neutrophils may also prolong injury repair via pro-inflammatory signalling (Pizza *et al.* 2005; Heredia *et al.* 2013). Neutrophil accumulation may suggest that older muscle is undergoing tissue remodelling, or is subject to impaired reparative responses compared to the younger participants. A hallmark of skeletal muscle ageing is an impaired reparative response to damage (McCormick & Vasilaki, 2018), and it is possible that an accumulation of muscle neutrophils contribute towards this impairment.

A striking observation from the present study was the profound increase in the expression of CD140a on progenitor cells in skeletal muscle and adipose tissue. CD140a is a marker of adipocyte progenitors that has been extensively characterized *in vivo* (Berry & Rodeheffer, 2013). Increased CD140a surface expression in adipose tissue, in the absence of an increase in the absolute cell counts of CD45−CD31−CD34+ progenitor cells, as well as in the absence of obesity, is unexpected. In murine models of obesity, CD140a+ adipocyte progenitors are selectively recruited to facilitate adipose tissue expansion (Lee *et al.* 2012). Therefore, ageing could induce a similar response which facilitates the redistribution of adipose tissue towards the abdomen that occurs with advancing age in humans (Palmer & Kirkland, 2016). Alternatively, the increase in adipose tissue progenitor cell CD140a expression may reflect an ongoing fibrotic response, possibly in response to the observed increase in adipocyte

size in the older participants (Iwayama *et al.* 2015). We have also reported a substantial increase in skeletal muscle progenitor cell CD140a expression in the older participants. In skeletal muscle, CD140a+ progenitors can differentiate into fibro-adipogenic progenitor cells, driving tissue fibrosis (Dani & Pfeifer, 2017). Increased muscle fibrosis is a fundamental factor in the process of sarcopenia, and one which CD140a+ progenitor cells may contribute towards (Uezumi *et al.* 2010; McCormick & Vasilaki, 2018). Thus, CD140a up-regulation in skeletal muscle during ageing might represent an early stage of fibro-adipogenic progenitor cell commitment that has downstream implications for the onset of sarcopenia, even in healthy, active ageing. Future work should look to clarify the precise implications of the striking age-related observed changes to progenitor cells in both muscle and adipose tissue.

In parallel to differences in the adipose tissue SVF, differences in adipocyte secretory functions were observed. Notable differences in circulating adipokines were shown in the present study, with significantly higher adiponectin and adipsin concentrations in older individuals. In humans, adiponectin increases with age and may present a survival advantage in healthy, long-lived individuals (Atzmon *et al.* 2008). Given the protective potential of adiponectin on metabolic and inflammatory health (Ouchi & Walsh, 2007), coupled with its positive relationship with physical activity status (Simpson & Singh, 2008), increased adiponectin in healthy older individuals may represent an adaptive phenotype that contributes to the maintenance of healthy ageing. Adipsin has recently been proposed as a regulator of experimental inflammatory arthritis, in mice, by preventing joint infiltration of neutrophils (Li *et al.* 2019). Therefore, increased circulating/adipose-derived adipsin may represent a normal biological ageing process that has not been reported previously, which may theoretically contribute to other age-associated diseases, such as arthritis.

In the present study, key proteins involved in the insulin signalling and glucose uptake were considerably lower in the adipose tissue of older individuals. However, there were no differences in these proteins in skeletal muscle between groups, and there were no differences in whole-body metabolic control in response to a mixed-meal tolerance test. The loss of insulin signalling protein content in adipose tissue, but not mRNA, may be secondary to increased adipose tissue inflammation (Hotamisligil, 2006; Chen *et al.* 2015). One mechanism through which this insulin desensitization occurs is by inactivating signal transduction downstream of IRS1. In response to a supraphysiological dose of insulin in the present study, isolated adipocytes exhibited no differences in the phosphorylation of Akt at serine 473. Although the total protein levels of some of the proteins involved in the insulin signalling cascade leading to GLUT4 translocation were lower in adipose tissue from older individuals, our *in vitro* adipocyte experiments suggest that proximal signalling events in adipocytes in response to stimulation with insulin might not be impacted. Further studies using lower/physiological concentrations of insulin and GLUT4 translocation experiments would be necessary to address this point. There were no differences in skeletal muscle insulin signalling protein content between groups. One explanation for these results might be the maintenance of a physically active lifestyle by the older individuals recruited in this study, preventing a decline in skeletal muscle insulin signalling with ageing (Short *et al.* 2003). Indeed, a previous study reported skeletal muscle GLUT4 protein content to be negatively correlated with age in men and women recruited without the inclusions requirement to be physical active (Houmard *et al.* 1995). The maintenance of muscle insulin signalling, coupled with a high ratio of muscle mass to adipose tissue mass, even with ageing, may explain the maintenance of whole-body glucose and insulin responses to the mixed-meal test in older participants. These observations emphasize the role of skeletal muscle in maintaining metabolic control even when other tissues such as adipose tissue show signs of insulin insensitivity and metabolic dysfunction. Future work should aim to investigate whether there are differences in the time scale of metabolic changes in adipose tissue and those observed in skeletal muscle and at the whole-body level; for example, via the use of tissue-specific arterio-venous differences in response to specific metabolic challenges.

One key strength of this research was the selection and recruitment of healthy, non-obese, and active older individuals with similar physical activity and body composition to a carefully-matched young comparator group. It is well established that overweight and/or physical inactivity profoundly affects ageing (Batsis & Villareal, 2018; Mahmassani *et al.* 2019). However, there are several limitations of the present work. We recruited males from the same geographical region and similar ethnic background, and whether the results would differ in other groups such as females warrants investigation. Indeed, aged female mouse adipose tissue CD8+ T-cells display greater activation and IFN-γ, TNF-α and granzyme B production than age-matched males (Ahnstedt *et al.* 2018). Further, although the present study isolated confounding lifestyle factors associated with ageing from biological factors driven by ageing *per se*, given that the prevalence of inactivity and obesity increases with advancing age, the results might not be representative of 'typical' ageing (Ogden *et al.* 2013; Townsend *et al.*, 2015). The present study does not examine the impact of ageing in older old people (e.g. >75 years), although our findings represent a major step forward in understanding given that the only other pre-

vious report of the impact of ageing in human adipose tissue is limited to a specific population of Pima Indians aged up to 45 years (Ortega Martinez de Victoria *et al.* 2009). Of course, the matching of young and older groups in terms of physical activity and adiposity will be even more challenging as the age gap between comparator groups is expanded. We should also acknowledge that the present findings are cross-sectional and we do not know how these observations might change over time. However, establishing cause and effect in human ageing is of course extremely technically challenging.

In conclusion, adipose tissue and skeletal muscle show marked immunometabolic changes with ageing in healthy adults, including a 2-fold increase in inflammatory T-cells, pronounced secretion of inflammatory mediators, activation of inflammatory signalling pathways and impaired insulin signalling. These age-associated changes to tissues were highly tissue-specific with very little commonality between cellular, protein and transcriptomic differences in adipose tissue and skeletal muscle in the same individuals. Moreover, the differences observed in adipose tissue and skeletal muscle with ageing were much more pronounced than those observed in systemic circulation. Thus, ageing appears to exert tissue-specific changes, at a local level, which may represent key tissue-specific remodelling events and early hallmarks of ageing that precedes systemic changes.

References

Abuzakouk M, Feighery C & O'Farrelly C (1996). Collagenase and dispase enzymes disrupt lymphocyte surface molecules. *J Immunol Methods* **194**, 211–216.

Ahnstedt H, Roy-O'Reilly M, Spychala MS, Mobley AS, Bravo-Alegria J, Chauhan A, Aronowski J, Marrelli SP & McCullough LD (2018). Sex differences in adipose tissue CD8+ T cells and regulatory T cells in middle-aged mice. *Front Immunol* **9**, 659.

Atzmon G, Pollin TI, Crandall J, Tanner K, Schechter CB, Scherer PE, Rincon M, Siegel G, Katz M, Lipton RB, Shuldiner AR & Barzilai N (2008). Adiponectin levels and genotype: a potential regulator of life span in humans. *J Gerontol A Biol Sci Med Sci* **63**, 447–453.

Bapat SP, Myoung Suh J, Fang S, Liu S, Zhang Y, Cheng A, Zhou C, Liang Y, LeBlanc M, Liddle C, Atkins AR, Yu RT, Downes M, Evans RM & Zheng Y (2015). Depletion of fat-resident Treg cells prevents age-associated insulin resistance. *Nature* **528**, 137–141.

Barberi L, Scicchitano BM, De Rossi M, Bigot A, Duguez S, Wielgosik A, Stewart C, McPhee J, Conte M, Narici M, Franceschi C, Mouly V, Butler-Browne G & Musaro A (2013). Age-dependent alteration in muscle regeneration: the critical role of tissue niche. *Biogerontology* **14**, 273–292.

Batsis JA & Villareal DT (2018). Sarcopenic obesity in older adults: aetiology, epidemiology and treatment strategies. *Nature Rev Endocrinol* **14**, 513–537.

Bergström J, Hermansen L, Hultman E & Saltin B (1967). Diet, Muscle Glycogen and Physical Performance. *Acta Physiol Scand* **71**, 140–150.

Berry R & Rodeheffer MS (2013). Characterization of the adipocyte cellular lineage in vivo. *Nat Cell Biol* **15**, 302–308.

Betts JA, & Thompson D (2012). Thinking outside the bag (not necessarily outside the lab). *Med Sci Sports Exerc* **44**, 2040.

Brigger D, Riether C, van Brummelen R, Mosher KI, Shiu A, Ding Z, Zbären N, Gasser P, Guntern P, Yousef H, Castellano JM, Storni F, Graff-Radford N, Britschgi M, Grandgirard D, Hinterbrandner M, Siegrist M, Moullan N, Hofstetter W, Leib SL, Villiger PM, Auwerx J, Villeda SA, Wyss-Coray T, Noti M & Eggel A (2020). Eosinophils regulate adipose tissue inflammation and sustain physical and immunological fitness in old age. *Nat Metabol* **2**, 688–702.

Brooks GA, Butte NF, Rand WM, Flatt J-P & Caballero B (2004). Chronicle of the Institute of Medicine physical activity recommendation: how a physical activity recommendation came to be among dietary recommendations. *Am J Clin Nutr* **79**, 921S.

Camell CD, Günther P, Lee A, Goldberg EL, Spadaro O, Youm Y-H, Bartke A, Hubbard GB, Ikeno Y, Ruddle NH, Schultze J & Dixit VD (2019). Aging induces an Nlrp3 inflammasome-dependent expansion of adipose B cells that impairs metabolic homeostasis. *Cell Metabol* **30**, 1024-1039.e6.

Chen L, Chen R, Wang H & Liang F (2015). Mechanisms linking inflammation to insulin resistance. *Intl J Endocrinol* **2015**, 1.

Cook RD (1977). Detection of influential observation in linear regression. *Technometrics* **19**, 15–18.

Cunningham F, Achuthan P, Akanni W, Allen J, Amode MR, Armean IM, Bennett R, Bhai J, Billis K, Boddu S, Cummins C, Davidson C, Dodiya KJ, Gall A, Girón CG, Gil L, Grego T, Haggerty L, Haskell E, Hourlier T, Izuogu OG, Janacek SH, Juettemann T, Kay M, Laird MR, Lavidas I, Liu Z, Loveland JE, Marugán JC, Maurel T, McMahon AC, Moore B, Morales J, Mudge JM, Nuhn M, Ogeh D, Parker A, Parton A, Patricio M, Abdul Salam AI, Schmitt BM, Schuilenburg H, Sheppard D, Sparrow H, Stapleton E, Szuba M, Taylor K, Threadgold G, Thormann A, Vullo A, Walts B, Winterbottom A, Zadissa A, Chakiachvili M, Frankish A, Hunt SE, Kostadima M, Langridge N, Martin FJ, Muffato M, Perry E, Ruffier M, Staines DM, Trevanion SJ, Aken BL, Yates AD, Zerbino DR & Flicek P (2019). Ensembl 2019. *Nucleic Acids Res* **47**, D745–D751.

Dalle S, Rossmeislova L & Koppo K (2017). The Role of Inflammation in Age-Related Sarcopenia. *Front Physiol* **8**, 1045.

Dani C & Pfeifer A (2017). The complexity of PDGFR signaling: regulation of adipose progenitor maintenance and adipocyte-myofibroblast transition. *Stem Cell Investig* **4**, 28-28.

Delmonico MJ, Harris TB, Visser M, Park SW, Conroy MB, Velasquez-Mieyer P, Boudreau R, Manini TM, Nevitt M, Newman AB & Goodpaster BH (2009). Longitudinal study of muscle strength, quality, and adipose tissue infiltration. *Am J Clin Nutr* **90**, 1579–1585.

Duffaut C, Zakaroff-Girard A, Bourlier V, Decaunes P, Maumus M, Chiotasso P, Sengenes C, Lafontan M, Galitzky J & Bouloumie A (2009). Interplay between human adipocytes and T lymphocytes in obesity: CCL20 as an adipochemokine and T lymphocytes as lipogenic modulators. *Arterioscler Thromb Vasc Biol* **29**, 1608–1614.

Fantuzzi G (2005). Adipose tissue, adipokines, and inflammation. *J Allergy Clin Immunol* **115**, 911–919; quiz 920.

FAO/ WHO/ UNU. (2005). Human energy requirements: report of a joint FAO/ WHO/ UNU Expert Consultation. *Food Nutr Bull.* **26**(1).

Franceschi C, Garagnani P, Parini P, Giuliani C & Santoro A (2018). Inflammaging: a new immune–metabolic viewpoint for age-related diseases. *Nat Rev Endocrinol* **14**, 576–590.

Frankish A, Diekhans M, Ferreira A-M, Johnson R, Jungreis I, Loveland J, Mudge JM, Sisu C, Wright J, Armstrong J, Barnes I, Berry A, Bignell A, Carbonell Sala S, Chrast J, Cunningham F, Di Domenico T, Donaldson S, Fiddes IT, García Girón C, Gonzalez JM, Grego T, Hardy M, Hourlier T, Hunt T, Izuogu OG, Lagarde J, Martin FJ, Martínez L, Mohanan S, Muir P, Navarro FCP, Parker A, Pei B, Pozo F, Ruffier M, Schmitt BM, Stapleton E, Suner M-M, Sycheva I, Uszczynska-Ratajczak B, Xu J, Yates A, Zerbino D, Zhang Y, Aken B, Choudhary JS, Gerstein M, Guigó R, Hubbard TJP, Kellis M, Paten B, Reymond A, Tress ML & Flicek P (2018). GENCODE reference annotation for the human and mouse genomes. *Nucleic Acids Res* **47**, D766–D773.

Frasca D & Blomberg BB (2017). Adipose tissue inflammation induces B cell inflammation and decreases B cell function in aging. *Front Immunol* **8**, 1003.

Frayn KN (1983). Calculation of substrate oxidation rates in vivo from gaseous exchange. *J Appl Physiol Respir Environ Exerc Physiol* **55**, 628–634.

Friedewald WT, Levy RI & Fredrickson DS (1972). Estimation of the concentration of low-density lipoprotein cholesterol in plasma, without use of the preparative ultracentrifuge. *Clin Chem* **18**, 499–502.

Girousse A, Gil-Ortega M, Bourlier V, Bergeaud C, Sastourne-Arrey Q, Moro C, Barreau C, Guissard C, Vion J, Arnaud E, Pradere JP, Juin N, Casteilla L & Sengenes C (2019). The release of adipose stromal cells from sub-cutaneous adipose tissue regulates ectopic intramuscular adipocyte deposition. *Cell Rep* **27**, 323-333.e5.e325.

Gustafson MP, Lin Y, Maas ML, Van Keulen VP, Johnston PB, Peikert T, Gastineau DA & Dietz AB (2015). A method for identification and analysis of non-overlapping myeloid immunophenotypes in humans. *PloS One* **10**, e0121546–e0121546.

Han SJ, Glatman Zaretsky A, Andrade-Oliveira V, Collins N, Dzutsev A, Shaik J, Morais da Fonseca D, Harrison OJ, Tamoutounour S, Byrd AL, Smelkinson M, Bouladoux N, Bliska JB, Brenchley JM, Brodsky IE & Belkaid Y (2017). White adipose tissue is a reservoir for memory T cells and promotes protective memory responses to infection. *Immunity* **47**, 1154-1168.e6 e1156.

Heredia JE, Mukundan L, Chen FM, Mueller AA, Deo RC, Locksley RM, Rando TA & Chawla A (2013). Type 2 innate signals stimulate fibro/adipogenic progenitors to facilitate muscle regeneration. *Cell* **153**, 376–388.

Holman GD, Kozka IJ, Clark AE, Flower CJ, Saltis J, Habberfield AD, Simpson IA & Cushman SW (1990). Cell surface labeling of glucose transporter isoform GLUT4 by bis-mannose photolabel. Correlation with stimulation of glucose transport in rat adipose cells by insulin and phorbol ester. *J Biol Chem* **265**, 18172–18179.

Hosack DA, Dennis G, Jr., Sherman BT, Lane HC & Lempicki RA (2003). Identifying biological themes within lists of genes with EASE. *Gen Biol* **4**, R70–R70.

Hotamisligil GS (2006). Inflammation and metabolic disorders. *Nature* **444**, 860–867.

Houmard JA, Weidner MD, Dolan PL, Leggett-Frazier N, Gavigan KE, Hickey MS, Tyndall GL, Zheng D, Alshami A & Dohm GL (1995). Skeletal muscle GLUT4 protein concentration and aging in humans. *Diabetes* **44**, 555.

Huang da W, Sherman BT & Lempicki RA (2009*a*). Bioinformatics enrichment tools: paths toward the comprehensive functional analysis of large gene lists. *Nucleic Acids Res* **37**, 1–13.

Huang da W, Sherman BT & Lempicki RA (2009*b*). Systematic and integrative analysis of large gene lists using DAVID bioinformatics resources. *Nat Protoc* **4**, 44–57.

Huang YP, Pechere JC, Michel M, Gauthey L, Loreto M, Curran JA & Michel JP (1992). In vivo T cell activation, in vitro defective IL-2 secretion, and response to influenza vaccination in elderly women. *J Immunol* **148**, 715–722.

Iwayama T, Steele C, Yao L, Dozmorov MG, Karamichos D, Wren JD & Olson LE (2015). PDGFRα signaling drives adipose tissue fibrosis by targeting progenitor cell plasticity. *Genes Dev* **29**, 1106–1119.

Kelly TL, Wilson KE & Heymsfield SB (2009). Dual energy X-ray absorptiometry body composition reference values from NHANES. *PloS One* **4**, e7038.

Kintscher U, Hartge M, Hess K, Foryst-Ludwig A, Clemenz M, Wabitsch M, Fischer-Posovszky P, Barth TF, Dragun D, Skurk T, Hauner H, Bluher M, Unger T, Wolf AM, Knippschild U, Hombach V & Marx N (2008). T-lymphocyte infiltration in visceral adipose tissue: a primary event in adipose tissue inflammation and the development of obesity-mediated insulin resistance. *Arterioscler Thromb Vasc Biol* **28**, 1304–1310.

Knights AJ, Vohralik EJ, Houweling PJ, Stout ES, Norton LJ, Alexopoulos SJ, Yik JJ, Mat Jusoh H, Olzomer EM, Bell-Anderson KS, North KN, Hoehn KL, Crossley M & Quinlan KGR (2020). Eosinophil function in adipose tissue is regulated by Krüppel-like factor 3 (KLF3). *Nat Comms* **11**, 2922.

Korf H, Boesch M, Feio-Azevedo R, Smets L, Vandecasteele R & van der Merwe S (2019). Depicting the landscape of adipose tissue-specific macrophages and their immuno-metabolic signatures during obesity. *Immunometabolism* **2**, e200001.

Lamble S, Batty E, Attar M, Buck D, Bowden R, Lunter G, Crook D, El-Fahmawi B & Piazza P (2013). Improved workflows for high throughput library preparation using the transposome-based nextera system. *BMC Biotechnol* **13**, 104.

Lee E-H, Itan M, Jang J, Gu H-J, Rozenberg P, Mingler MK, Wen T, Yoon J, Park S-Y, Roh JY, Choi CS, Park W-J, Munitz A & Jung Y (2018). Eosinophils support adipocyte maturation and promote glucose tolerance in obesity. *Sci Rep* **8**, 9894.

Lee Y-H, Petkova Anelia P, Mottillo Emilio P & Granneman James G (2012). In vivo identification of bipotential adipocyte progenitors recruited by β3-adrenoceptor activation and high-fat feeding. *Cell Metabol* **15**, 480–491.

Li Y, Zou W, Brestoff JR, Rohatgi N, Wu X, Atkinson JP, Harris CA & Teitelbaum SL (2019). Fat-produced adipsin regulates inflammatory arthritis. *Cell Rep* **27**, 2809-2816.e3.e2803.

Lopez-Otin C, Blasco MA, Partridge L, Serrano M & Kroemer G (2013). The hallmarks of aging. *Cell* **153**, 1194–1217.

Love MI, Huber W & Anders S (2014). Moderated estimation of fold change and dispersion for RNA-seq data with DESeq2. *Genome Biol* **15**, 550.

Lumeng CN, Liu J, Geletka L, Delaney C, Delproposto J, Desai A, Oatmen K, Martinez-Santibanez G, Julius A, Garg S & Yung RL (2011). Aging is associated with an increase in T cells and inflammatory macrophages in visceral adipose tissue. *J Immunol* **187**, 6208–6216.

Mahmassani ZS, Reidy PT, McKenzie AI, Stubben C, Howard MT & Drummond MJ (2019). Age-dependent skeletal muscle transcriptome response to bed rest-induced atrophy. *J Appl Physiol* **126**, 894–902.

Mancuso P & Bouchard B (2019). The impact of aging on adipose function and adipokine synthesis. *Front Endocrinol* **10**, 137.

Matthews DG, Altman P, Campbell P & Royston P (1990). Analysis of serial measurements in medical research. *Brit Med J* **300**, 230–235.

Matthews DR, Hosker JP, Rudenski AS, Naylor BA, Treacher DF & Turner RC (1985). Homeostasis model assessment: insulin resistance and beta-cell function from fasting plasma glucose and insulin concentrations in man. *Diabetologia* **28**, 412–419.

McCormick R & Vasilaki A (2018). Age-related changes in skeletal muscle: changes to life-style as a therapy. *Biogerontology* **19**, 519–536.

Ogden CL, Carroll MD, Kit BK & Flegal KM (2013). Prevalence of obesity among adults: United States, 2011–2012. *NCHS Data Brief* **131**, 1–8.

Ortega Martinez de Victoria E, Xu X, Koska J, Francisco AM, Scalise M, Ferrante AW, Jr. & Krakoff J (2009). Macrophage content in subcutaneous adipose tissue: associations with adiposity, age, inflammatory markers, and whole-body insulin action in healthy Pima Indians. *Diabetes* **58**, 385–393.

Ouchi N & Walsh K (2007). Adiponectin as an anti-inflammatory factor. *Clin Chim Acta* **380**, 24–30.

Palmer AK & Kirkland JL (2016). Aging and adipose tissue: potential interventions for diabetes and regenerative medicine. *Experiment Gerontol* **86**, 97–105.

Paradisi G, Smith L, Burtner C, Leaming R, Garvey WT, Hook G, Johnson A, Cronin J, Steinberg HO & Baron AD (1999). Dual energy X-ray absorptiometry assessment of fat mass distribution and its association with the insulin resistance syndrome. *Diabetes Care* **22**, 1310–1317.

Pérez LM, Pareja-Galeano H, Sanchis-Gomar F, Emanuele E, Lucia A & Gálvez BG (2016). 'Adipaging': Aging and obesity share biological hallmarks related to a dysfunctional adipose tissue. *J Physiol* **594**, 3187–3207.

Pertea M, Kim D, Pertea GM, Leek JT & Salzberg SL (2016). Transcript-level expression analysis of RNA-seq experiments with HISAT, StringTie and Ballgown. *Nature Protoc* **11**, 1650–1667.

Pertea M, Pertea GM, Antonescu CM, Chang T-C, Mendell JT & Salzberg SL (2015). StringTie enables improved reconstruction of a transcriptome from RNA-seq reads. *Nat Biotechnol* **33**, 290–295.

Pillon NJ, Bilan PJ, Fink LN & Klip A (2013). Cross-talk between skeletal muscle and immune cells: muscle-derived mediators and metabolic implications. *Am J Physiol Endocrinol Metabol* **304**, E453–E465.

Pizza FX, Peterson JM, Baas JH & Koh TJ (2005). Neutrophils contribute to muscle injury and impair its resolution after lengthening contractions in mice. *J Physiol* **562**, 899–913.

Reilly SM & Saltiel AR (2017). Adapting to obesity with adipose tissue inflammation. *Nat Rev Endocrinol* **13**, 633–643.

Short KR, Vittone JL, Bigelow ML, Proctor DN, Rizza RA, Coenen-Schimke JM & Nair KS (2003). Impact of aerobic exercise training on age-related changes in insulin sensitivity and muscle oxidative capacity. *Diabetes* **52**, 1888–1896.

Simpson KA & Singh MA (2008). Effects of exercise on adiponectin: a systematic review. *Obesity* **16**, 241–256.

Soro-Arnaiz I, Li QOY, Torres-Capelli M, Melendez-Rodriguez F, Veiga S, Veys K, Sebastian D, Elorza A, Tello D, Hernansanz-Agustin P, Cogliati S, Moreno-Navarrete JM, Balsa E, Fuertes E, Romanos E, Martinez-Ruiz A, Enriquez JA, Fernandez-Real JM, Zorzano A, De Bock K & Aragones J (2016). Role of mitochondrial complex IV in age-dependent obesity. *Cell Rep* **16**, 2991–3002.

Starnes T, Broxmeyer HE, Robertson MJ & Hromas R (2002). Cutting edge: IL-17D, a Novel Member of the IL-17 family, stimulates cytokine production and inhibits hemopoiesis. *J Immunol* **169**, 642.

Steffen BJ, Butcher EC & Engelhardt B (1994). Evidence for involvement of ICAM-1 and VCAM-1 in lymphocyte interaction with endothelium in experimental autoimmune encephalomyelitis in the central nervous system in the SJL/J mouse. *Am J Pathol* **145**, 189–201.

Sturn A, Quackenbush J & Trajanoski Z (2002). Genesis: cluster analysis of microarray data. *Bioinformatics* **18**, 207–208.

Sugiura T, Murakawa Y, Nagai A, Kondo M & Kobayashi S (1999). Fas and Fas ligand interaction induces apoptosis in inflammatory myopathies: CD4+ T cells cause muscle cell injury directly in polymyositis. *Arthritis Rheumatol* **42**, 291–298.

Talukdar S, Oh da Y, Bandyopadhyay G, Li D, Xu J, McNelis J, Lu M, Li P, Yan Q, Zhu Y, Ofrecio J, Lin M, Brenner MB & Olefsky JM (2012). Neutrophils mediate insulin resistance in mice fed a high-fat diet through secreted elastase. *Nat Med* **18**, 1407–1412.

Thompson D, Karpe F, Lafontan M & Frayn K (2012). Physical activity and exercise in the regulation of human adipose tissue physiology. *Physiol Rev* **92**, 157–191.

Tidball JG (2017). Regulation of muscle growth and regeneration by the immune system. *Nat Rev Immunol* **17**, 165–178.

Townsend N, Wickramasinghe K, Williams J, Bhatnagar P & Rayner M (2015). *Physical activity statistics*, ed. Foundation BH. London, UK.

Trapnell C, Roberts A, Goff L, Pertea G, Kim D, Kelley DR, Pimentel H, Salzberg SL, Rinn JL & Pachter L (2012). Differential gene and transcript expression analysis of RNA-seq experiments with TopHat and Cufflinks. *Nature Protoc* **7**, 562–578.

Travers RL, Motta AC, Betts JA, Bouloumie A & Thompson D (2015). The impact of adiposity on adipose tissue-resident lymphocyte activation in humans. *Int J Obes* **39**, 762–769.

Travers RL, Motta AC, Betts JA & Thompson D (2017). Adipose tissue metabolic and inflammatory responses to a mixed meal in lean, overweight and obese men. *Eur J Nutr* **56**, 375–385.

Trim W, Thompson D & Turner JE (2017). Adipose Tissue Dysfunction. In *Encyclopedia of Behavioral Medicine*, ed. Gellman M & Turner JR, pp. 1–5. Springer, New York, NY.

Trim W, Turner JE & Thompson D (2018). Parallels in immunometabolic adipose tissue dysfunction with ageing and obesity. *Front Immunol* **9**, 169.

Uezumi A, Fukada S, Yamamoto N, Takeda S & Tsuchida K (2010). Mesenchymal progenitors distinct from satellite cells contribute to ectopic fat cell formation in skeletal muscle. *Nat Cell Biol* **12**, 143–152.

Villalta SA, Rosenthal W, Martinez L, Kaur A, Sparwasser T, Tidball JG, Margeta M, Spencer MJ & Bluestone JA (2014). Regulatory T cells suppress muscle inflammation and injury in muscular dystrophy. *Sci Transl Med* **6**, 258ra142.

Walhin JP, Richardson JD, Betts JA & Thompson D (2013). Exercise counteracts the effects of short-term overfeeding and reduced physical activity independent of energy imbalance in healthy young men. *J Physiol* **591**, 6231–6243.

Watanabe Y, Nagai Y, Honda H, Okamoto N, Yanagibashi T, Ogasawara M, Yamamoto S, Imamura R, Takasaki I, Hara H, Sasahara M, Arita M, Hida S, Taniguchi Si, Suda T & Takatsu K (2019). Bidirectional crosstalk between neutrophils and adipocytes promotes adipose tissue inflammation. *FASEB J* **33**, 11821–11835.

Westerterp KR (2004). Diet induced thermogenesis. *Nutr Metabol* **1**, 5.

WHO (2011). *Waist circumference and waist–hip ratio report of a WHO expert consultation*, Geneva, 8–11 December 2008. Geneva, Switzerland.

Wu D, Ren Z, Pae M, Guo W, Cui X, Merrill AH & Meydani SN (2007*a*). Aging up-regulates expression of inflammatory mediators in mouse adipose tissue. *J Immunol* **179**, 4829–4839.

Wu H, Ghosh S, Perrard XD, Feng L, Garcia GE, Perrard JL, Sweeney JF, Peterson LE, Chan L, Smith CW & Ballantyne CM (2007*b*). T-cell accumulation and regulated on activation, normal T cell expressed and secreted upregulation in adipose tissue in obesity. *Circulation* **115**, 1029–1038.

Yang L, Froio RM, Sciuto TE, Dvorak AM, Alon R & Luscinskas FW (2005). ICAM-1 regulates neutrophil adhesion and transcellular migration of TNF-alpha-activated vascular endothelium under flow. *Blood* **106**, 584–592.

Yang W & Hu P (2018). Skeletal muscle regeneration is modulated by inflammation. *J Orth Transl* **13**, 25–32.

Yu Q, Xiao H, Jedrychowski MP, Schweppe DK, Navarrete-Perea J, Knott J, Rogers J, Chouchani ET & Gygi SP (2020). Sample multiplexing for targeted pathway proteomics in aging mice. *Proc Natl Acad Sci USA* **117**, 9723.

Additional information

Data availability statement

Sequencing data sets associated with this work are available from GenBank, accession code GSE175495. All remaining datasets generated during the current study are available in the University of Bath Data Repository (https://doi.org/10.15125/BATH-00806).

Competing interests

The authors declare that they have no competing interests.

Author contributions

Funding

Acknowledgements

Keywords

Supporting information

Additional supporting information may be found online in the Supporting Information section at the end of the article.

Statistical Summary Document